A Design of Compact Planar Low-Pass Filter for Harmonics and Spurious Suppression

by Rui Li

Under Supervision of Prof. Dong Il Kim

Department of Radio Sciences and Engineering

in the Graduate School

of the

Korea Maritime University

February 2007

A Design of Compact Planar Low-Pass Filter for Harmonics and Spurious Suppression

by Rui Li

A dissertation submitted in partial satisfaction of the requirements for degree of

Doctor

in Radio Sciences and Engineering in the Graduate School of the

Korea Maritime University.

Committee in charge

Prof.	Se-Mo Chung
Prof.	Young Sup Ahn
Prof.	Kyeong-Sik Min
Prof.	Ki-Moon Kim
Prof.	Dong Il Kim

Contents

Nomenclature

C :	Capacitance
C_c :	Parasitic capacitance to each other
C_g :	Parasitic capacitance to ground
f :	Frequency
f_0 :	Center frequency
f_n :	Normalized frequency
L :	Self-inductance
M :	Mutual-inductance
Z_0 :	Characteristic impedance
Z_{oe} :	Even-mode characteristic impedance
Z_{oo} :	Odd-mode characteristic impedance
Z_I :	Image impedance
$[S]$	Scattering matrix
$[T]$:	Transfer matrix
$[Y]$:	Admittance matrix
$[Z]$:	Impedance matrix
β :	Propagation number
ε_0 :	Air dielectric constant
ε_r :	Relative dielectric constant
θ :	Electrical length
λ :	Wavelength
ω :	Angular frequency

List of Tables

List of Figures

Abstract

A Design of Compact Planar Low-Pass Filter for Harmonics and Spurious Suppression

Rui Li
Dept. of Radio Sciences & Engineering
Graduate School, Korea Maritime Univ.
Supervisor : Prof. Dong Il Kim, Ph. D

Low-pass filters are often employed in many communication systems to suppress harmonics and spurious signals, which demand compact size, low insertion loss, and high attenuation. The conventional low-pass filters, such as open-stub low-pass filters and stepped impedance low-pass filters can not meet the requirements for modern communication systems because of their large size and narrow stopband.

In this dissertation, a novel compact structure with three controllable finite attenuation poles at stopband was proposed. The new structure is composed of a pair of symmetrical parallel coupled-line and a capacitive load. With this configuration, three finite attenuation poles are available, which can improve the stopband characteristics of low-pass filters or the upper stopband performances of band-pass filters. The research method is based on transmission-line model for tuning the finite attenuation poles. In order to examine the feasibility of the proposed structure, the new type low-pass filter with broad stopband and sharp cutoff frequency response based on microstrip structure was

designed, fabricated, and measured. The experimental results of the fabricated circuit agree well with the simulation and analytical ones. In addition, a semi-lumped low-pass filter was designed, fabricated, and measured, which can suppress 2^{nd}, 3^{rd}, and 4^{th} harmonics. In addition, any of the unwanted signals can be eliminated using this design method by adjusting the electrical circuit parameters.

요 약

하모닉과 스퓨리어스 신호를 억제하기 위해 소형화 평면형 저역 통과 필터의 설계

Rui Li
학 교: 한 국 해 양 대 학 교
학 과: 전 파 공 학 과
지도교수: 김 동 일

하모닉과 스퓨리어스 신호를 억제하기 위해서 사용되는 저역통과필터는 많은 통신시스템에서 보다 작은 사이즈와, 낮은 사입손실, 그리고 저지 대역에서 높은 감쇠특성을 필요로한다. 그러나 개방 스터브 저역통과필터와 계단형 임피던스 저역통과필터와같은 종래의 저역통과필터는 현대 통신시스템에 대한 이러한 요구를 만족할 수 없다.

본 논문에서는 저지 대역에서 조절가능한 3개의 유한 감쇠 폴을 갖는 새로운 소형화된 회로를 제안하였으며 이 회로는 대칭적인 평행 결합선과 컨덴서로 구성되어 있다. 이 구조는 3개의 유한 감쇠 폴이 조절가능하기때문에 저지 대역필터의 저지대역의 특성과 통과 대역필터의 높은 저지대역 특성을 개선할 수 있다. 본 논문에서의 연구 방법은 전송선로 모델을 이용하여 유한 감쇠 폴의 위치를 조절하는 것이다. 제안된 회로의 가능성을 확인하기 위하여 마이크로 스트립 기판으로 넓은 저지 대역폭과 샤프한 차단 주파수 특성을 갖는 저역 통과 필터를 설계하고 제작한 후 주파수특성을 측정하여 시뮬레이션 결과와 비교한 결과, 측정결과와 시뮬레이션 결과는 잘 일

치함을 학인하고 있다. 다음으로, semi-lumped 저역 통과필터를 설계해서 제작 후 주파수 특성을 측정한 결과 2차, 3차, 그리고 4차 고조파 신호를 제거할 수 있었으며, 회로의 전기적인 파라미터를 조절해서 원하지 않은 신호를 제거할 수 있다.

CHAPTER 1 Introduction

The microwave region of the electromagnetic spectrum has certain properties. These enable microwave signals to propagate over long distances through the atmosphere under all but the most severe weather conditions. Both civilian and military applications abound, including radar, navigation, and the latest “hot application,” wireless communications. However, the microwave spectrum is a finite resource which must be divided according to frequency (see Fig. 1.1). And this is where microwave filters come in [1], [2]. Microwave filters are important components in a variety of electronic systems including cellular radios, satellite communications and radars [3], [4]. They are used to separate or combine different frequencies. Emerging applications such as wireless communications continue to challenge RF/microwave filters with ever more stringent requirements such as higher performance, small size, lighter weight, and more important factor-lower cost. The recent advances in novel materials and fabrication technologies, including high-temperature superconductors (HTS), low-temperature co-fired ceramics (LTCC) [5], monolithic microwave integrated circuits (MMIC), micro-electro-mechanic system (MEMS), and micromachining technology, have stimulated the rapid development of new microstrip and other filters for RF/Microwave applications [6].

RF & Microwave spectrums

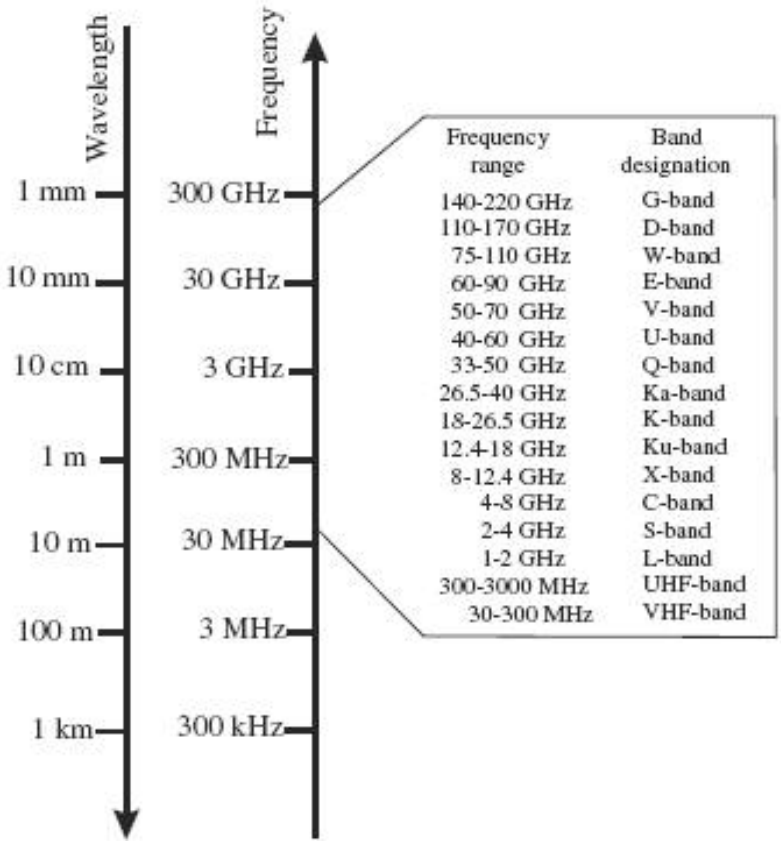

Fig. 1.1 RF/ Microwave spectrums.

There are several different classification methods for filters. It is well known that they can be divided into four types of filters in RF/Microwave system mainly in terms of frequency selectivity characteristics, such as Low-Pass Filter (LPF), High-Pass Filter (HPF), Band-Pass Filter (BPF), and Band-Stop Filter (BSF). Their representative frequency responses are shown in Fig. 1.2. And following the different implementation methods of filters, there are

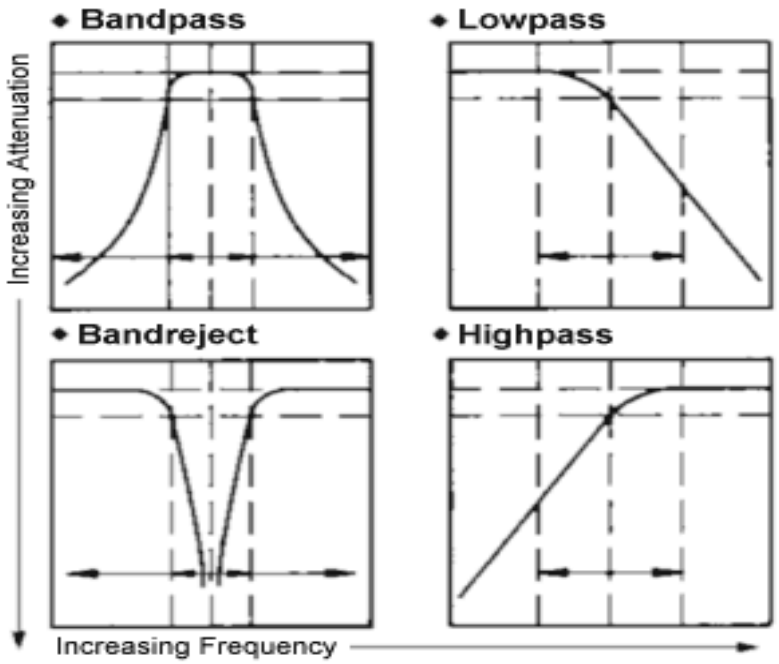

Fig. 1.2 Classification in terms of frequency responses.

two main kinds, such as lumped-elements and distributed-elements filters. Lumped-elements filters are frequently applied in low-frequency band because the wavelength of the operation signal will be comparable to the size of the lumped-elements itself, whereas the distributed-elements filters can be used in high-frequency band extending to decades and hundreds of GHz (giga hertz). As a typical representative, the RF filters based on microstrip-line structures have some excellent advantages such as low cost, easy to fabricate and integrate, and so on. That is why this kind of filters finds a wide application in modern communication systems.

1.1 Background and purpose

A. Harmonic signals

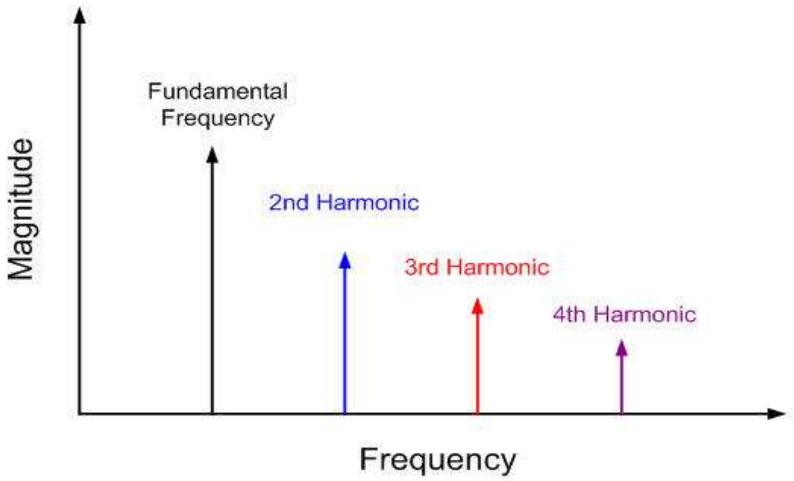

Fig. 1.3 Graphic description of harmonics.

As is well known, a harmonic is a signal or wave whose frequency is an integral (whole-number) multiple of the frequency of some reference signal or wave. The term can also refer to the ratio of the frequency of such a signal or wave to the frequency of the reference signal or wave (see Fig. 1.3) [7]. Up to now, harmonics are usually generated in active components, such as PA (power amplifier), LNA (low noise amplifier), mixer, and so on (see Fig. 1.4) because of the transistors being used in these components [8], and these active components are necessary to transceivers. Therefore, a study on harmonics is great significant to modern communication systems.

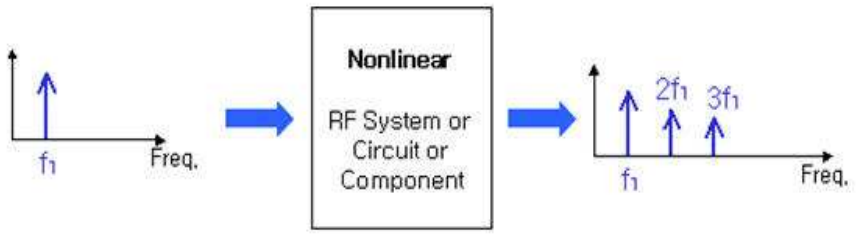

Fig. 1.4 Harmonics generation.

However, there are two roles harmonics play in transceiver system. One is the specific harmonics of RF signals can be utilized to be a source of an oscillator and frequency synthesizer. For example, a harmonic frequency of 300-Hz developed on a 60-Hz system is the fifth harmonic (5 x 60 Hz = 300 Hz). On the contrary, the presentations of harmonics cause some problems to communication systems, such as harmonics distortions. Harmonic signals can reduce level of efficiency of any communication systems. For examples, the

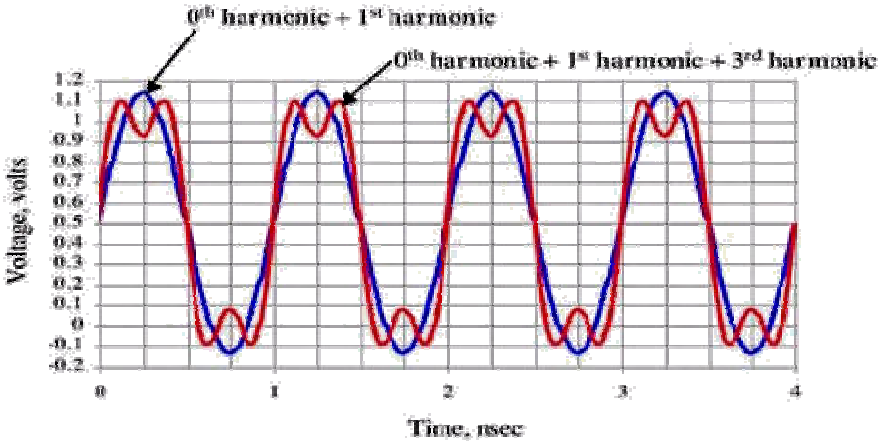

Fig. 1.5 Harmonics distortion description.

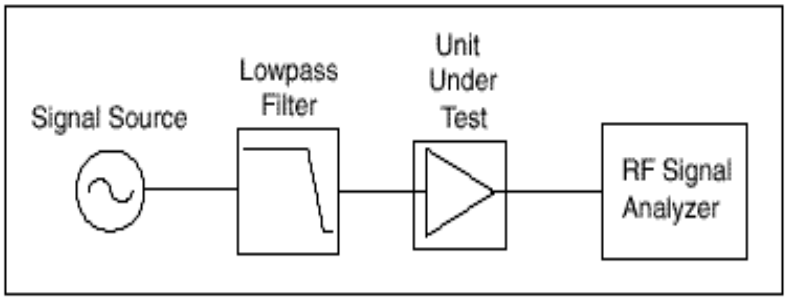

Fig. 1.6 Test system for harmonics.

fundamental signal, which is a sine wave in the time domain with a frequency of 1 GHz, when it is added by the 1st and 3rd harmonics, the result in the time domain is not a standard sine wave any more. This is shown in Fig. 1.5. In this case, the harmonics influence the quality of the communication systems strongly, especially signal integrity [9].

A typical setup to perform a harmonic distortion measurement is shown in Fig. 1.6 above. A low-pass or band-pass filter passes the fundamental signal while suppressing its harmonics. This setup injects a very clean sinusoidal signal into the device under test (DUT). Any harmonic content at the DUT output is assumed to be generated by the DUT instead of the source [10].

Harmonic distortion can be effectively reduced in any real world system through the use of low-pass or band-pass filtering.

B. Spurious signals

With the exception of harmonic signals, there are other signals which have to be eliminated in communication systems, to be called spurious signals. Here, the spurious signals mentioned above refer to non-harmonics spurious signals. They appear usually in the planar circuits based on strip-lines, microstrip-lines, slot-lines and coplanar structure due to the intrinsic characteristics of the planar structures. However, they have valuable features as electromagnetic wave filters: a simple structure, a small size, and the capability of wide application to various devices. Moreover, the most attractive feature of microstrip-line, strip-line or coplanar-line resonators is that they can be easily integrated with active circuits such as MMICs, because they are manufactured by photolithography of metalized film on a dielectric substrate [11],[12].

Particularly, microstrip-line filters, as very popular and important components, have been employed widely in communication

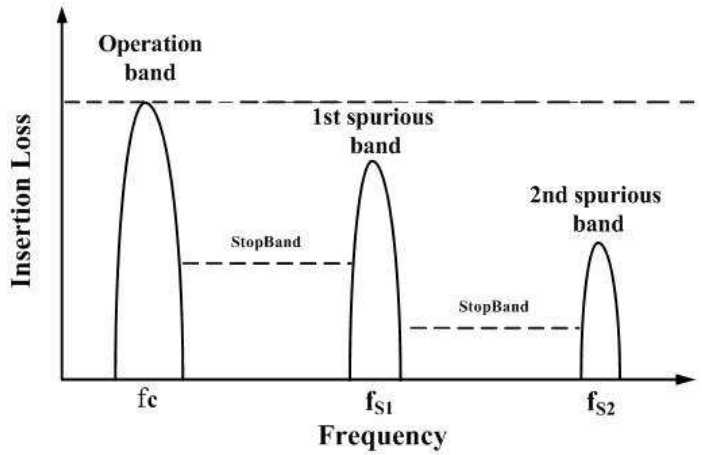

Fig. 1.7 Spurious band description.

systems. Generally, this kind of filters utilizes the resonators of λ/4, λ/2 and SIR (Stepped-Impedance Resonator) [6]. As is well known, these filters have the periodic frequency responses. Therefore, one of the significant disadvantages is that the first spurious passband of the conventional type of filters appears so closely and strongly that the rejection of the upper stopband is worse than that of the lower stopband as shown in Fig. 1.7. Sometimes, the upper stopband rejection may be as bad as 10 dB, especially in case of wide bandwidth filters. Therefore, the selectivity performance of filters will be decreased to a large extent.

C. Solutions to these two problems

Present research on microwave filters is very active because of the continuous demands of high-performance circuits from modern communication and electronic systems. To suppress harmonics and spurious signals, many researchers have taken a lot of effort. For instances, K. H. Yi and B. K. Kang employed open-stubs of λ/4n wavelength into conventional Wilkinson power divider for nth harmonics suppression [13], W. H. Tu and K. Chang proposed a compact second harmonic-suppressed band-stop and band-pass filters [14], and so on. In a different view, C. Quendo and E. Rius integrated an optimized low-pass filter in a band-pass filter for out-of –band improvement [15]. A semi-lumped low-pass filter for harmonics and spurious suppression was proposed by Jyh-Wen Sheen [16].In addition, PBG (Photonic Band-Gap) and DGS (Defected Ground Structure) techniques have been widely used to improve stopband characteristics of filters [17], [18], like a design of the novel coupled-line band-pass filter using DGS with wide stopband performance proposed by J. S.

Park and J. S. Yun. All the methods mentioned-above require complicated analysis and optimization processes. The simplest method for harmonics and spurious suppression is applying a low-pass filter into the integrated circuits.

As is well known, the low-pass filters are often employed in many communication systems to suppress harmonic and spurious signals [19], with the demand for compact size, easy-to-integrate, low insertion loss, wide out-of-band, and high attenuation level. The conventional low-pass filters, such as open-circuited stub low-pass filters and stepped impedance low-pass filters can not meet the requirements for modern communication systems because of their large size and narrow stopband. For sharper cutoff and high attenuation at stopband, the order of the stepped-impedance low-pass filter must be very high [1], [2], thereby the circuit size and insertion loss will be increased. In literature, many design approaches have been proposed to improve the low-pass filter's performance. The low-pass filters using PBG and DGS structures can improve the skirt characteristic and provide wide and deep stopband as compared with the conventional low-pass filters, however, fabrication process becomes difficult and EMC/EMI problems will be produced due to the defected ground. A low-pass filter using multiple cascaded hairpin resonators that can provide sharp cutoff frequency responses with low passband insertion loss has been demonstrated in [20], [21]. However, this type of design approach is a little complicated and just used to synthesize some parts of available prototype low-pass filters. In addition, W. H Tu and K. Chang have proposed a compact microstrip low-pass filter with sharp rejection characteristics [22]. This kind of filters can provide two transmission zeros through stopband.

In this dissertation, a novel and more compact structure fabricated on microstrip line structure is proposed and a new type of low-pass filter based on this structure, which consists of a pair of symmetrical parallel coupled-line and a capacitive load, is developed. Its equivalent circuits are extracted and the details of extraction process for the equivalent circuits are depicted in this work. The proposed structure demonstrates many attractive features: simple and compact structure, low passband insertion loss, broad stopband, sharp skirt characteristic and three controllable transmission zeros which can suppress the harmonics and specific spurious signals.

1.2 Research contents

Chapter 1 briefly presents classification of filters and discusses the importance of the suppression for harmonics and spurious signals. In addition, the former research achievements in this region are proposed in this chapter.

In chapter 2, the basic theory of low-pass filters are introduced briefly. The structure is proposed and its equivalent circuit extracted from Chebyshev low-pass filter prototype is derived and discussed in detail. Simulating by using ADS simulator (Advanced Design System), the skirt characteristics and rejection bandwidth of out-of-band can be optimized. And a low-pass filter designed by this proposed method is fabricated and measured. However, by comparing the simulated and measured results, we find a shortcoming about this equivalent.

Chapter 3 focuses on the problem found out in chapter 2, and based on this point, the equivalent circuit proposed in chapter 2 is improved by changing the circuit topology to depict the frequency responses of the proposed compact structure more exactly.

In chapter 4, the circuit proposed in this thesis was been analyzed by using even-odd mode method, and from this analysis results, it is found that there are three transmission zeros through the whole stopband which can be controllable to suppress specific harmonics and spurious signals. Based on this design method, a low-pass filter has been designed, fabricated and measured for suppressing the 2^{nd}, the 3^{rd}, and the 4^{th} harmonics signals. By comparing the simulated and measured results, the feasibility of this approach can be confirmed.

Chapter 5 is the conclusion of this research work and presents a future plan.

CHAPTE 2 Compact Low-Pass Filters

2.1 Basic theory for a low-pass filter design

As is well-known, there are generally four types of low-pass filter prototypes applied in RF/Microwave circuits, such as, Butterworth-type (also called maximally flat), Chebyshev-type, Bessel-type, and Elliptic function type, etc [3]. All these types have distinguishing characteristics, respectively. Therefore, we should select an appropriate type prior to design work according to the required filter's specifications, and the design process is as shown in Fig. 2.1.

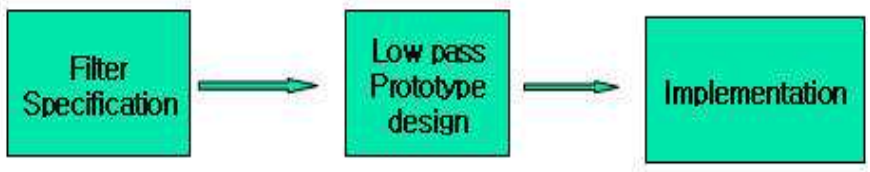

Fig. 2.1 Low-pass filters implementation.

To better understand the operation mechanism of low-pass filters, and how to select an appropriate low-pass filter's type we need for some real-world applications, therefore some comparable features of the above-mentioned four types of low-pass filters are discussed as following:

A. Butterworth filters

The **Butterworth filter** is one type of electronic filter design. It is designed to have a frequency response which is as flat as mathematically possible in the passband. Another name for them is 'maximally flat magnitude' filters. The Butterworth type filter was first described by the British engineer Stephen Butterworth in his paper "On the Theory of Filter Amplifiers" [23]. The frequency response of the Butterworth filter is maximally flat (has no ripples) in the passband, and rolls off towards zero in the stopband. When viewed on a logarithmic Bode plot, the response slopes off linearly towards negative infinity. As shown in Fig. 2.2, its network topology and frequency responses are presented.

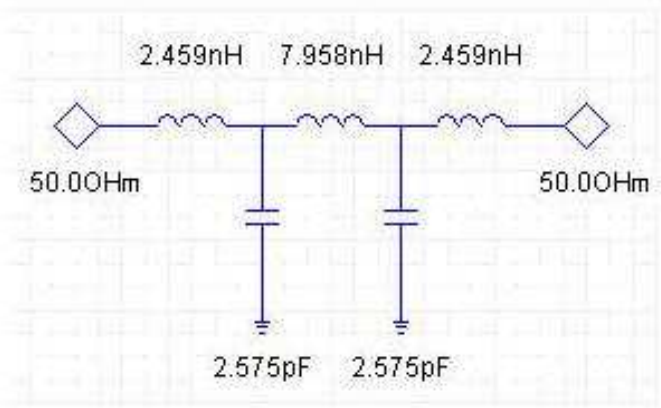

(a)

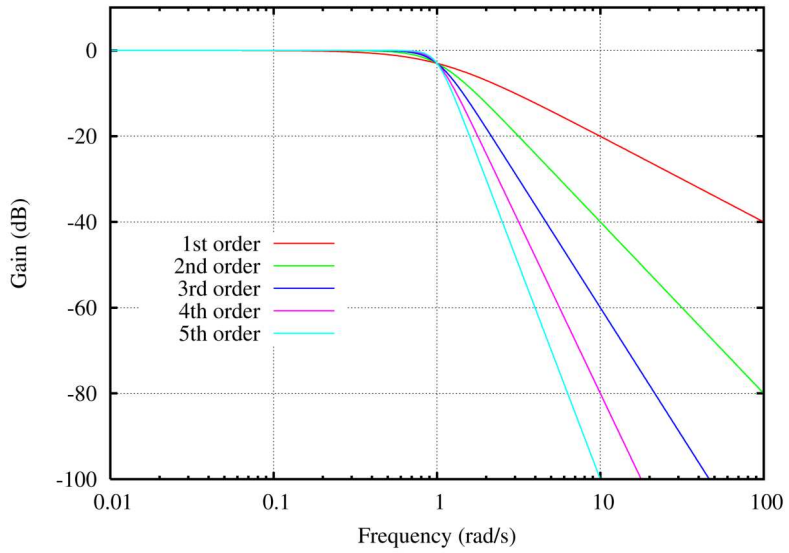

(b)

Fig. 2.2 (a) Network topology (for 5th order at 2 GHz) and (b) comparison of frequency responses of Butterworth low-pass filters with different order.

For a first-order filter, the response rolls off at −6 dB per octave (−20 dB per decade). (All first-order filters, regardless of name, are actually identical and so have the same frequency response.) For a second-order Butterworth filter, the response decreases at −12 dB per octave, a third-order at −18 dB, and so on. Butterworth filters have a monotonically decreasing magnitude function with ω. The Butterworth is the only filter that maintains this same shape for higher orders (but with a steeper decline in the stopband) whereas other varieties of filters (Bessel, Chebyshev, elliptic) have different shapes at higher orders.

Compared with a Chebyshev Type I/Type II filter or an elliptic filter, the Butterworth filter has a slower roll-off, and thus will require a higher order to implement a particular stopband specification. However, Butterworth filter will have a more linear phase response in the passband than the Chebyshev Type I/Type II and elliptic filters.

B. Chebyshev filters

Chebyshev filters, are widely-used a type of filters having a steeper roll-off and more passband ripple than Butterworth filters. Chebyshev filters have the property that they minimise the error between the idealised filter characteristic and the actual over the range of the filter, but with ripples in the passband. This type of filters is named in honor of Pafnuty Chebyshev because their mathematical characteristics are derived from Chebyshev polynomials [3].

They are divided into two types: Chebyshev Type I and Chebyshev Type II with respect to the different network topologies. Type I are the most common Chebyshev filters. The order of a Chebyshev filter is equal to the number of reactive components. Type II is also known as inverse Chebyshev, this type is less common because it does not roll off as fast as type I, and requires more components. It has no ripple in the passband, but does have ripple in the stopband. Because of the passband ripple inherent in Chebyshev filters, filters which have a smoother response in the passband but a more irregular response in the stopband are preferred for some applications.

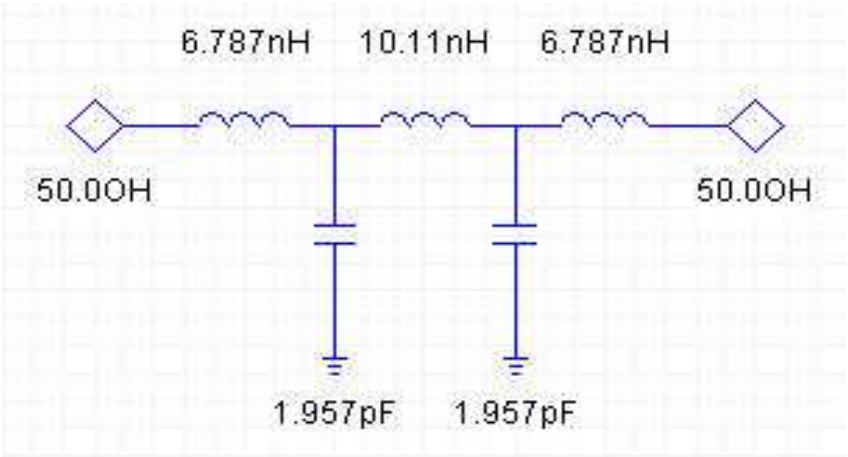

(a)

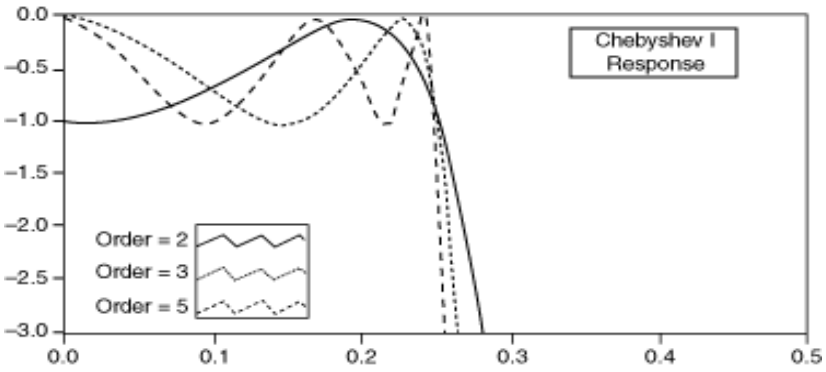

(b)

Fig. 2.3 (a) Network topology (for 5th order and 0.5 dB ripple at 2 GHz) and (b) comparison of frequency responses of Type I Chebyshev low-pass filters with different order.

As shown in Fig. 2.3, the network topology and frequency responses are demonstrated.

C. Elliptic filters

An **elliptic filter** (also known as a **Cauer filter**) is a filter with equiripple behavior in both the passband and the stopband. For a specified minimum ripple in the pass band and the stop band, no other filter of equal order can do better than an elliptic filter. It minimizes the maximum error in both bands, as opposed to a Chebyshev filter which exhibits equal and minimized ripple in the pass band, or the inverse Chebyshev filter which exhibits equal and minimized ripple in the stop band. In addition, the Elliptic Filter contains a sharp cut off, high group delay, and greatest stop band attenuation. Like the Chebyshev Type I Filter, the Elliptic pass band attenuation is defined to be the same value as the pass band ripple amplitude. However, Filter Solutions allows the user the option of selecting any pass band attenuation in dB's that will define the filters cut off frequency.

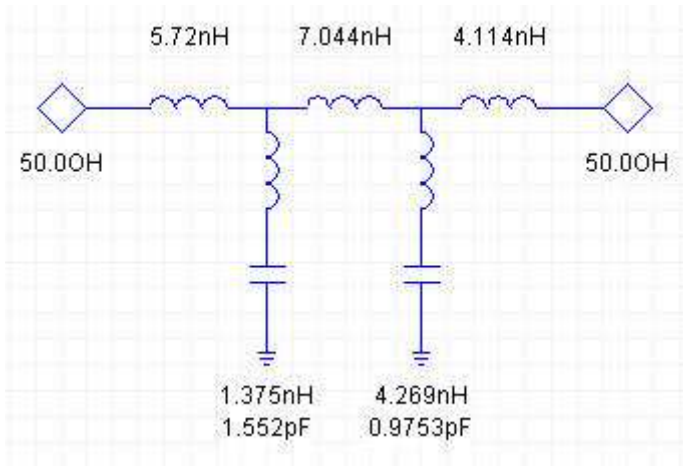

(a)

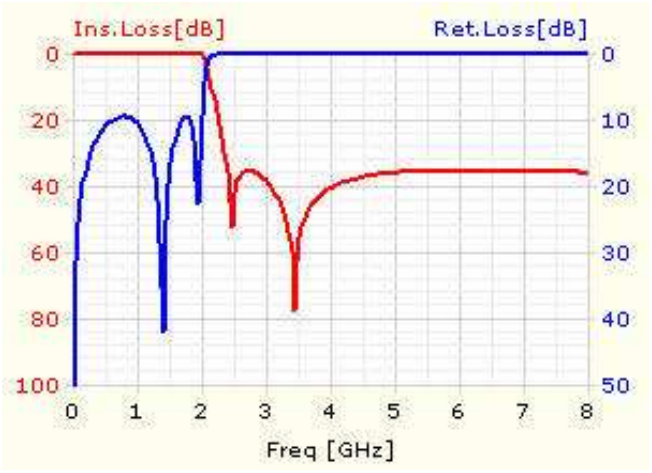

(b)

Fig. 2.4 (a) Network topology (for 5th order with 0.5 dB ripple at 2 GHz) and (b) comparison of frequency responses of elliptic-function low-pass filters.

In order to have a sharp cutoff frequency response, the elliptic-function low-pass filters have been employed widely and frequently. The frequency responses and network topology are shown in Fig. 2.3.

D. Bessel filters

In electronics and signal processing, a **Bessel filter** is a variety of linear filter with a maximally flat group delay (linear phase response). Bessel filters are often used in audio crossover systems. Analog Bessel filters are characterized by almost constant group delay across the entire passband, thus preserving the wave shape of filtered signals in the passband. Here, the network topology is similar as Butterworth prototype low-pass fiter, and the frequency responses are ommited.

E. Brief comparison description

Based on above-mentioned four types of low-pass filters, we should draw a conclusion about how to select an appropriate type for specific application?

Here are some images showing a comparison of frequency-responses and group-delay characteristics between different low-pass filters with the same number of coefficients:

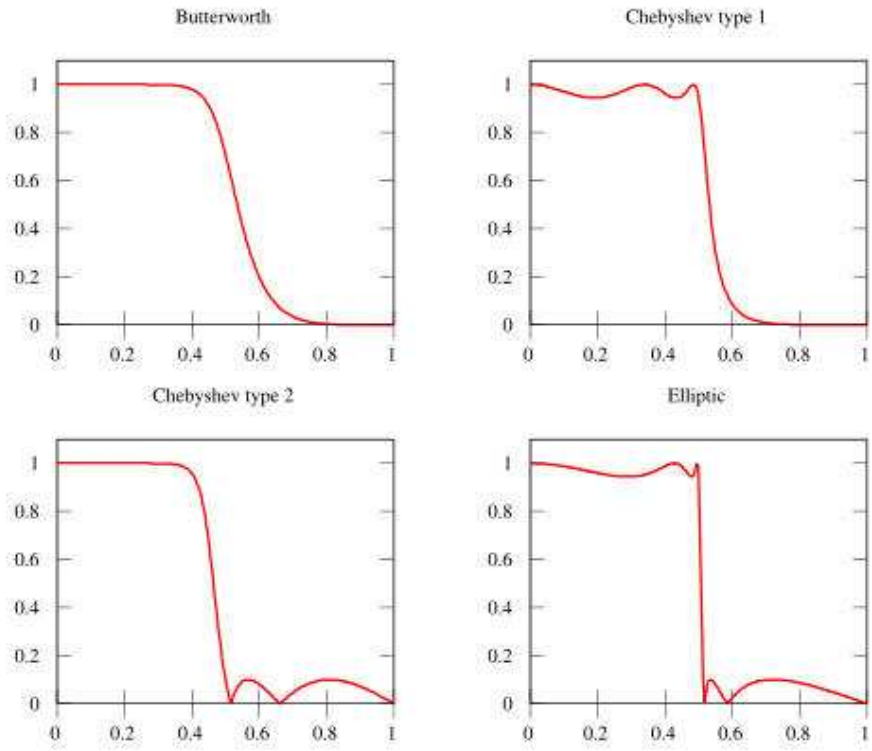

(a)

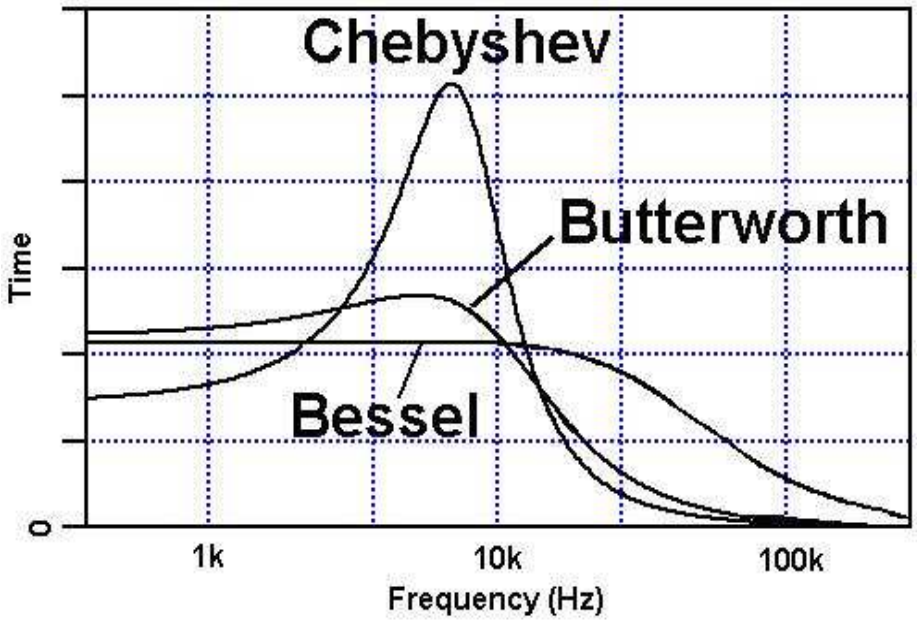

(b)

Fig. 2.5 (a) Frequency responses and (b) group delay characteristics.

By comparing the frequency responses and group-delay characteristics of these different low-pass filters, the advantages and disadvantages are showing as following:

— Butterworth maximally flat magnitude

Advantages:

Maximally flat magnitude response in the pass-band.
Good group-delay performance than Chebyshev.

Rate of attenuation better than Bessel.

Disadvantages:

Wide transition band and poor attenuation level.

— Chebyshev equal ripple magnitude

Advantages:

Better rate of attenuation beyond the pass-band than Butterworth.

Disadvantages:

Ripple in pass-band, high insertion-loss than Butterworth type.
High group delay than Butterworth and Bessel types.

And Chebyshev type II (inverse Chebyshev type) has equi-ripple in stop-band but not in pass-band.

— Bessel - also called Thomson

Advantages:

Best group-delay characteristics than other types.

Disadvantages:

Slower initial rate of attenuation beyond the pass-band than Butterworth, Chebyshev and Elliptic-function types.

— Elliptic-function

Advantages:

Best attenuation rate in transition and high attenuation level than other types.

Disadvantages:

Poor group-delay characteristic than Chebyshev type.

More lumped-elements required dude to its complicated network topology.

By enumerating the advantages and disadvantages above, a brief flow-chart is made to easily select an appropriate type for a specific application, as shown in Fig. 2.6 below.

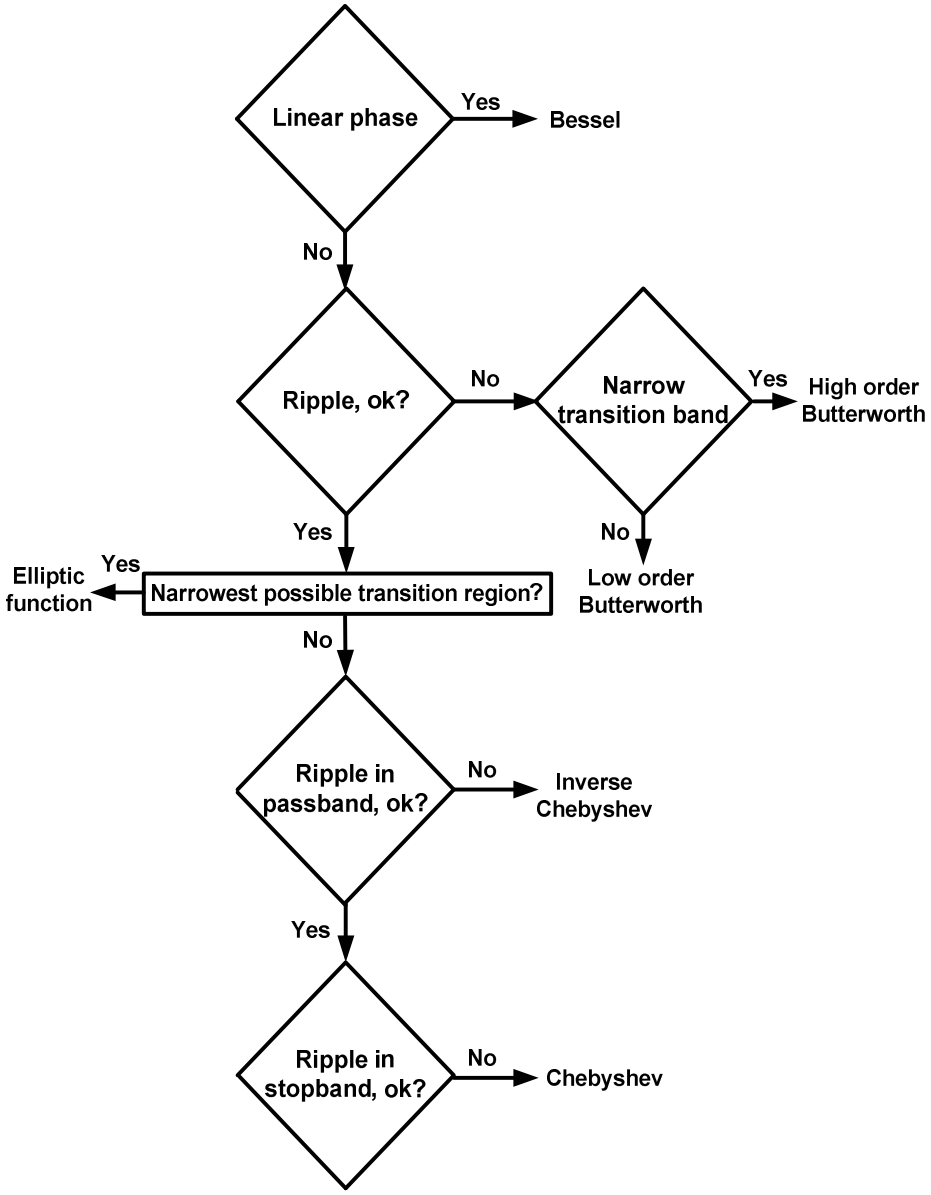

Fig. 2.6 Flow chart for filter-type selecting.

2.2 Conventional microstrip low-pass filters

As is well known, RF filters based on microstrip structure have some excellent advantages such as low cost, easy to fabricate and integrate, and so on. Therefore, the low-pass filters based on microstrip structure have been the main emphasis of researches [2].

The conventional low-pass filters based on microstrip line structure include several types, such as stepped-impedance low-pass filter, open-stub low-pass filter, and quasi-elliptic function low-pass filter, etc. As follows, they are introduced below, including their circuit layout and corresponding frequency responses.

The stepped-impedance and open-stub low-pass filters can be transformed from Chebyshev, Butterworth, and Bessel prototype. As shown in Fig. 2. 7, the prototype circuit comprised of lumped-elements and the planar circuits based on microstrip line structure are demonstrated.

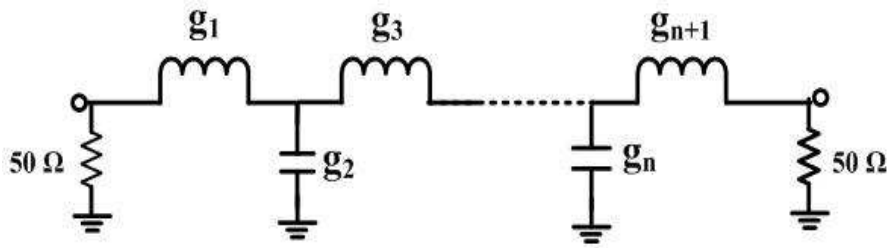

(a)

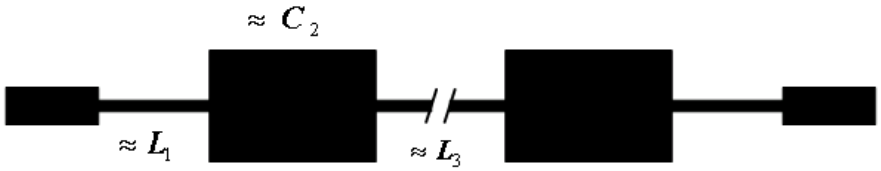

(b)

Fig. 2.7 (a) General network topology using lumped-elements and (b) stepped-impedance low-pass filter based on microstrip line structure.

where the physical parameters of the stepped-impedance low-pass filters can be approximately derived. As shown in Fig. 2.8, the conventional transmission line can be represented by *T*-type and *Π*-type network comprised of lumped-elements inductors and capacitors.

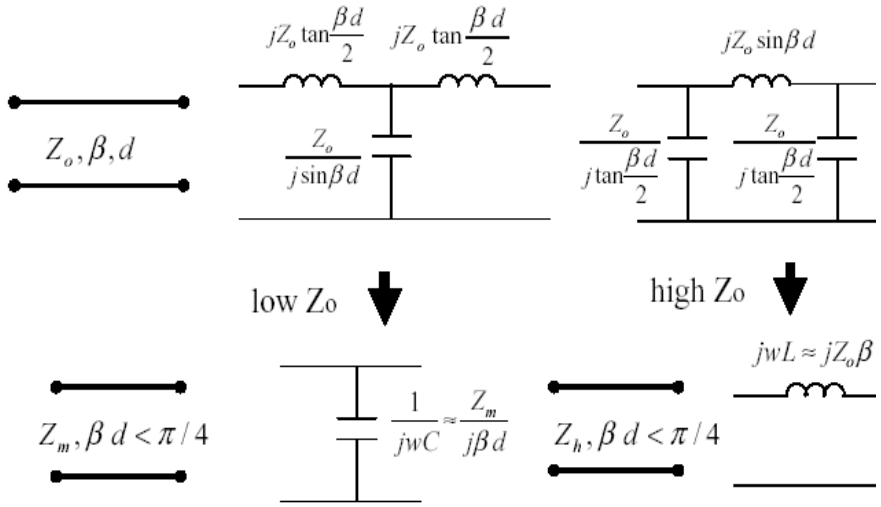

Fig. 2.8 Transform from lumped-elements to planar components.

In the case of low-impedance, the series-inductors in *T*-type can be omitted due to the low value of the characteristic impedance; therefore the low-impedance line can be used to be a capacitor approximately. And in the case of high-impedance, the shunt-capacitors can be neglected because of the high impedance-value, the transformation processes and the formulas are shown in Fig. 2.9.

where $g_0, g_1 \ldots g_n$ are the elements values in prototype circuits, they can be found in the authorities' published tables, Z_0 is the characteristic impedance, $L_1, C_1 \ldots C_n$ represent the lumped-elements values, λ means the wavelength of the operation frequency, and l_L, l_C are the length of the high- and low-impedance lines, f means the central operation frequency.

The previous stepped-impedance low-pass filter realizes the shunt-capacitors of the low-pass prototype as low impedance lines in the transmission path. An alternative realization of a shunt capacitor is to use an open-circuited stub subject o where the term on the left-hand side is the susceptance of shunt-capacitor, whereas the term on the right-hand side represents the input susceptance of open-circuited stub, which has characteristic impedance Z_0 and a physical length l that is

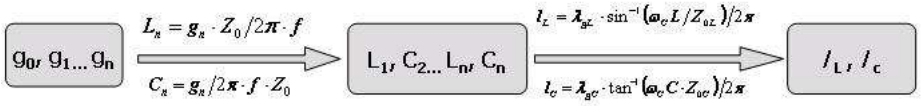

Fig. 2.9 Transformation processes and formulas.

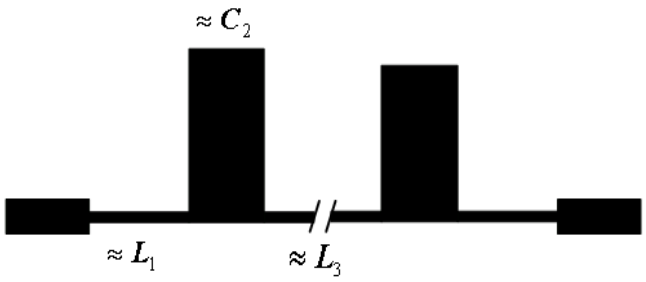

Fig. 2.10 Open-stub low-pass filter based on microstrip line.

smaller than a quarter of guided wavelength λ_g. Therefore, the following type of low-pass filter based on microstrip line structure is referred to as open-stub low-pass filter, and its layout is as shown in Fig. 2.10. Also, the transformation process and formulas are all the same with the stepped-impedance low-pass filters as shown in Fig. 2.8~2.9.

The next planar low-pass filter based on microstrip structure is very popular in RF/microwave circuit because of its sharp skirt-characteristics and high attenuation level. That is elliptic-function low –pass filter whose layout can be derived from the corresponding elliptic-function prototype, as shown in Fig. 2. 11.

All the three types of the conventional microstrip low-pass filters cannot meet the demands for modern microwave circuit. If we want to realize a low-pass filter with high-attenuation and sharp transition-band, the lumped-elements will be six or more. In this case, however, the circuit size will be so large that the integration with other RF components becomes difficult. So the compact planar filters with

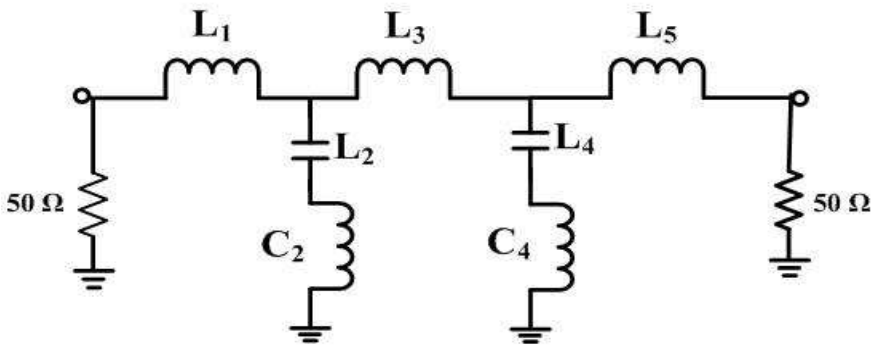

(a)

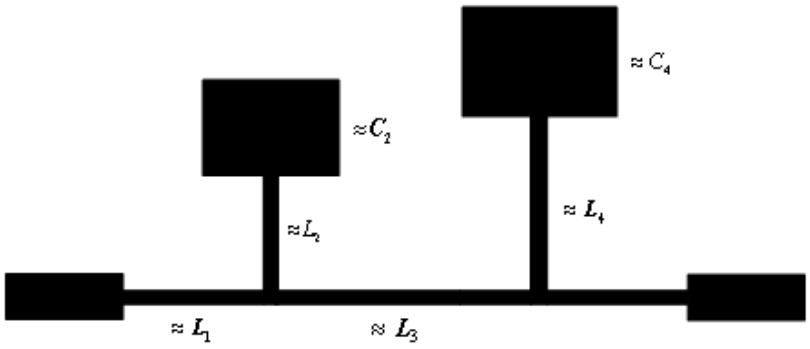

(b)

Fig. 2.11 (a) Prototype network and (b) circuit layout of elliptic-function low-pass filter based on microstrip line structure.

high-performances, easy-to-integrate, low cost, low insertion-loss and high attenuation level at out-of-band have to be developed to satisfy the increasing requirements.

2.3 Compact planar structure

2.3.1 Low-pass filter with compact planar structure

Recently, some compact low-pass filters have been proposed in published papers, including the compact low-pass filter using the cascaded stepped-impedance resonators by L. H. Hsieh and K. Chang in Jan. 2003, a compact microstrip low-pass filter with sharp rejection using inter-digital capacitor reported by W. H. Tu and K. Chang in June, 2005, a representative design of the low-pass filter using the novel microstrip defected ground structure proposed by D. Ahn, J. S. Park, C. S. Kim, J. Kim, Y. Qian, and T. Itoh in Aug. 2005.

In this paper, we proposed a new compact microstrip low-pass filter with broad stopband and sharp skirt characteristics. The philosophy of the structure behind this novel microstrip low-pass filter is simple as it is comprised of a pair of parallel coupled-line and an open-stub. With this configuration, a finite attenuation pole near the stopband cutoff frequency is available, and the notch frequency can be well controlled by adjusting the circuit parameters. The design formulas are derived by using an equivalent-circuit model of a parallel coupled transmission line. In order to validate the feasibility of the proposed design method, a 3-order Chebyshev low-pass filter with 0.01-dB ripple is designed, fabricated, and measured. Experimental results agree well with the simulation and analytical results.

2.3.2 Proposed compact structure

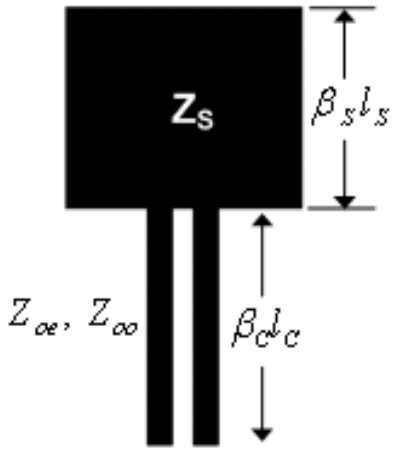

Fig. 2.12 Layout of the proposed compact low-pass filter.

Fig. 2.12 shows the layout of our proposed low-pass filter. This low-pass filter consists of an open-stub with the length of *ls* and a pair of parallel coupled-line with the length of *lc*. Z_S is the characteristic impedance of the open-stub, while *Zoe* and *Zoo* represent the even- and odd-mode impedance of the parallel coupled-line, respectively.

To analyzer this compact structure simply, we firstly assume that the structure is lossless and the width of the feeding lines is negligible. Under these assumptions, this type of compact structure can be divided into two sections, namely open-stub section and parallel coupled-line section.

A. Modeling of the open-stub

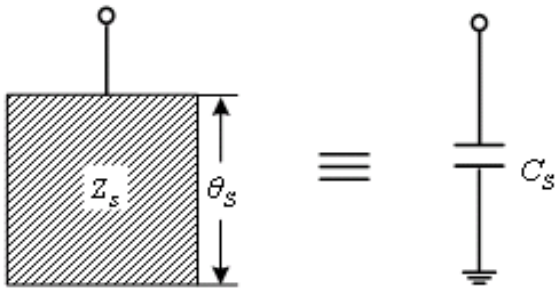

Fig. 2.13 Equivalent circuit of an open-stub.

The open-stub section is modeled as an equivalent capacitor, as shown in Fig. 2. 13. The open-stub can be considered as a quasi-MIM capacitor, and the equivalent capacitance can be obtained from [24]:

$$\boldsymbol{Y_{in}^{S} = jY_S} \tan \boldsymbol{\theta_S} \tag{2.1}$$

where $\boldsymbol{Y_{in}^{S}}$ is an input admittance from the starting point of the open-stub, $\boldsymbol{Y_S}$ is the characteristic impedance of the open-stub transmission line, and $\boldsymbol{\theta_S}$ is the electrical length of the open-stub.

For a load capacitor shown in the right of Fig. 2.13, its input admittance can be calculated as following:

$$\boldsymbol{Y_{in}^{C} = j\omega_0 C_S} \tag{2.2}$$

where Y_{in}^{C} means the input admittance of the load capacitor, ω_0 is operation frequency, C_S represents the capacitance value.

Therefore, by equalizing the right parts of Eqn. (1) and (2), the relationship between the open-stub and the load capacitor can be obtained, as shown in Eqn. (3) below:

$$C_S = \frac{Ys \cdot \tan\theta_S}{\omega_0} \tag{2.3}$$

For a parallel-plate capacitor, the capacitance can be calculated by Eqn. (4) [25]:

$$C = \varepsilon_0 \varepsilon_r \frac{Wl}{d} = \frac{\varepsilon_r 10^{-15}}{36\pi} \frac{Wl}{d} (F) \tag{2.4}$$

where ε_r is the relative dielectric constant; *W, l,* and *d* are the width, length, and thickness of the parallel-plate capacitor, respectively.

B. Modeling of the parallel coupled-line with its far-end shorted

Comparing with the modeling of an open-stub, a parallel coupled-line with its far-end shorted is a little complicated. First of all, as depicted in Fig. 2.14, the symmetrical parallel coupled-line is modeled as a transmission line section.

The relevant parameters can be obtained from [3]:

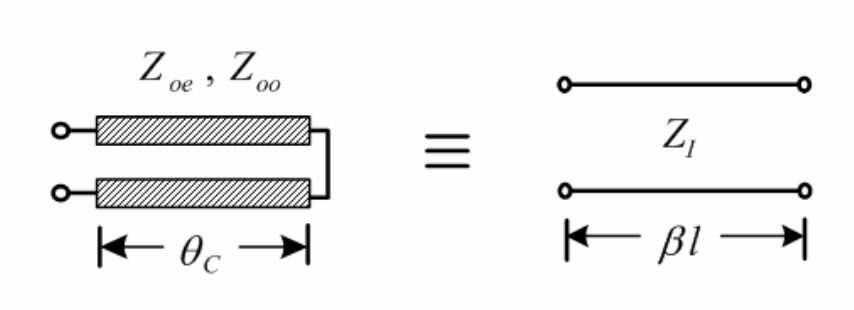

Fig. 2.14 Equivalent circuit of a symmetrical parallel coupled-line with its far-end shorted.

$$Z_I = \sqrt{Z_{oe} \cdot Z_{oo}} \tag{2.5}$$

$$\tan(\beta l) = \frac{2\sqrt{Z_{oe} \cdot Z_{oo}}}{Z_{oe}\cot\theta_c - Z_{oo}\tan\theta_c} \tag{2.6}$$

$$\cos(\beta l) = \frac{\frac{Z_{oe}}{Z_{oo}} - \tan^2\theta_c}{\frac{Z_{oe}}{Z_{oo}} + \tan^2\theta_c} \tag{2.7}$$

where Z_I is the image impedance, βl is the image propagation function for the transmission line section. In fact, for the case of a uniform transmission line, the image impedance of the line is also its characteristic impedance and the image propagation function is also the electrical length of the line.

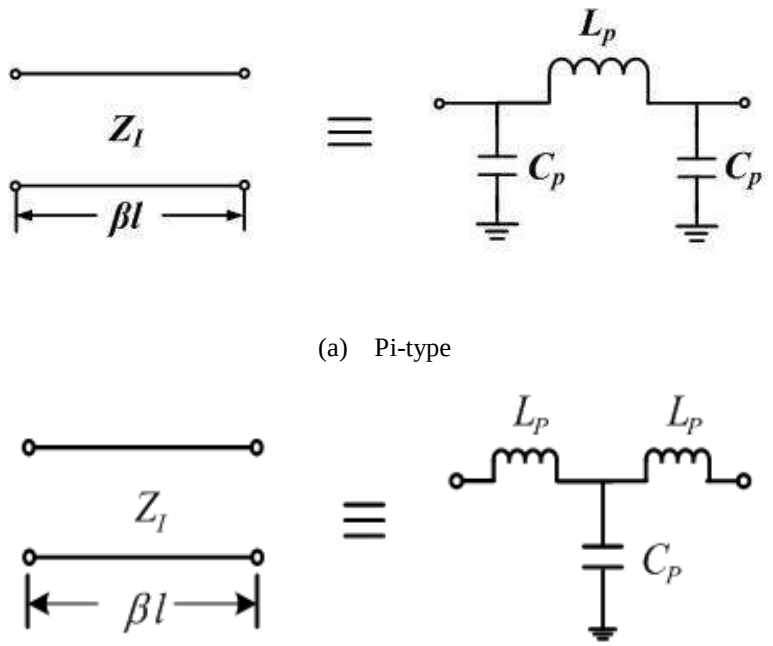

Fig. 2.15 Equivalent circuit of a transmission line section.

From the basic theory of network-transformations, the transmission line section can be transformed into two-types of network comprised of lumped elements, such as *Pi*-type and *T*-type [26], [27], as shown in Fig. 2.15. In this work, we choose the *T*-type as the one we need here to simplify the analysis process.

For a lossless single transmission line section with a length of *l*, its *ABCD* matrix is given by

$$\begin{bmatrix} A & B \\ C & D \end{bmatrix} = \begin{bmatrix} \cos(\beta l) & jY_I \sin(\beta l) \\ jY_I \sin(\beta l) & \cos(\beta l) \end{bmatrix} \tag{2.8}$$

where $Y_I = 1/Z_I$ is the characteristic admittance of the single line. The *ABCD* matrix of the equivalent *T*-type network is

$$\begin{bmatrix} A_T & B_T \\ C_T & D_T \end{bmatrix} = \begin{bmatrix} 1 + Z_L Y_C & Z_L (2 + Z_L Y_C) \\ Y_C & 1 + Z_L Y_C \end{bmatrix} \tag{2.9}$$

where $Z_L = j\omega L_P$, $Y_c = j\omega C_P$, and ω is the angular operation frequency, and L_P and C_P are the equivalent inductance and capacitance of the single transmission line. Comparing (2.8) and (2.9), the L_P and C_P can be obtained as

$$C_P = \frac{Y_I \cdot \sin(\beta l)}{\omega} \tag{2.10}$$

and

$$L_P = \frac{Z_I \cdot \tan(\frac{\beta l}{2})}{\omega} \tag{2.11}$$

Furthermore, by combining the equivalent-circuit models of the open-stub and the symmetrical parallel coupled-line, a whole equivalent-circuit in terms of lumped elements *L* and *C* can be achieved, as shown in Fig. 2.16, where the shunt capacitance is the sum of C_S and C_P.

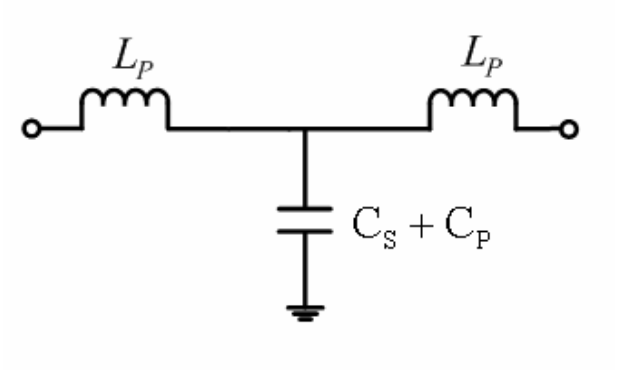

Fig. 2.16 A whole equivalent circuit of the open-stub modeling circuit and the parallel coupled-line modeling circuit.

Table 2.1 Element values for Chebyshev low-pass fiters with 0.01 dB ripple

VALUE OF n	g_1	g_2	g_3	g_4	g_5	g_6	g_7	g_8	g_9	g_{10}	g_{11}
0.01 db ripple											
1	0.0960	1.0000									
2	0.4488	0.4077	1.1007								
3	0.6291	0.9702	0.6291	1.0000							
4	0.7128	1.2003	1.3212	0.6476	1.1007						
5	0.7563	1.3049	1.5773	1.3049	0.7563	1.0000					
6	0.7813	1.3600	1.6896	1.5350	1.4970	0.7098	1.1007				
7	0.7969	1.3924	1.7481	1.6331	1.7481	1.3924	0.7969	1.0000			
8	0.8072	1.4130	1.7824	1.6833	1.8529	1.6193	1.5554	0.7333	1.1007		
9	0.8144	1.4270	1.8043	1.7125	1.9057	1.7125	1.8043	1.4270	0.8144	1.0000	
10	0.8196	1.4369	1.8192	1.7311	1.9362	1.7590	1.9055	1.6527	1.5817	0.7446	1.1007
0.1 db ripple											
1	0.3052	1.0000									
2	0.8430	0.6220	1.3554								
3	1.0315	1.1474	1.0315	1.0000							
4	1.1088	1.3061	1.7703	0.8180	1.3554						
5	1.1468	1.3712	1.9750	1.3712	1.1468	1.0000					
6	1.1681	1.4039	2.0562	1.5170	1.9029	0.8618	1.3554				
7	1.1811	1.4228	2.0966	1.5733	2.0966	1.4228	1.1811	1.0000			
8	1.1897	1.4346	2.1199	1.6010	2.1699	1.5640	1.9444	0.8778	1.3554		
9	1.1956	1.4425	2.1345	1.6167	2.2053	1.6167	2.1345	1.4425	1.1956	1.0000	
10	1.1999	1.4481	2.1444	1.6265	2.2253	1.6418	2.2046	1.5821	1.9628	0.8853	1.3554

2.3.3 Compact Low-pass filter implementation

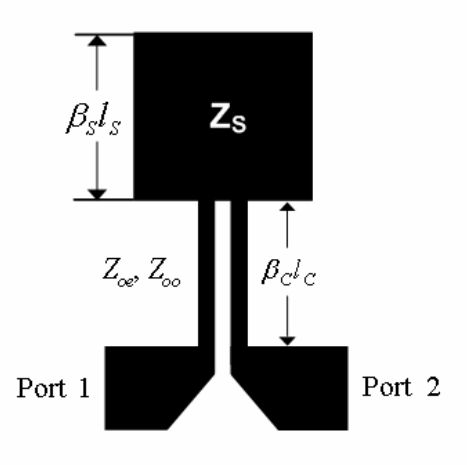

(a)

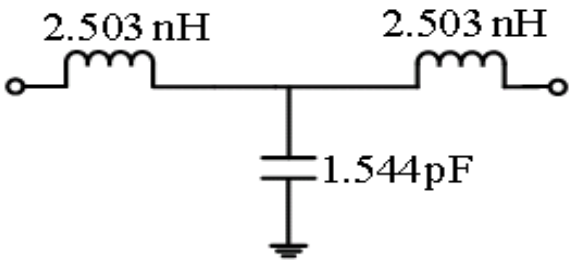

(b)

Fig. 2.17 Low-pass filter using one-unit. (a) Layout. (b) equivalent circuit.

Up to now, the proposed compact structure and its equivalent analysis process have been discussed above. It is obviously that the whole equivalent circuit has an identical network topology as the conventional low-pass filter prototype. Therefore, we will design a low-pass filter based on the published table of a Chebyshev prototype low-pass filter as shown in Table I below.

A. Low-pass filter using one-unit structure

To validate the proposed design approach, a 3-order 0.01-dB ripple Chebyshev low-pass prototype filter with a 3-dB cutoff at 2 GHz is synthesized. By using the 0.01-dB ripple one, we can obtain a very low insertion-loss through the passband.

Fig. 2.17 shows the geometry and equivalent circuit of the Chebyshev low-pass filter using one-unit structure. And the equivalent inductance L_P and the sum of the equivalent capacitances C_P are 2.503 *nH* and 1.544 *pF*, respectively, and the physical dimensions extracted by Eqn. (2.1) ~ (2.11) are shown in Table II. The low-pass filter is designed and fabricated on a 1.524 mm thick Taconic PCB with a relative dielectric constant of 3.5.

As shown in Table 2.2, the dimensions of the coupled-line are fixed, as the shorter the coupled-line is, the more difficult the fabrication becomes. Furthermore, we investigated the frequency responses of the proposed low-pass filter with different open-stub

Table 2.2 Physical dimensions of the proposed low-pass filter

No.	Parallel coupled-line (mm)	Open-stub		Effective area (mm × mm)
		Width (mm)	Length (mm)	
1	Width: 0.36	12.06	4.03	12.06 × 9.58
2	Space: 0.67	7.17	5.96	7.17 × 11.51
3	Length: 5.55	3.40	9.37	3.40 × 14.93

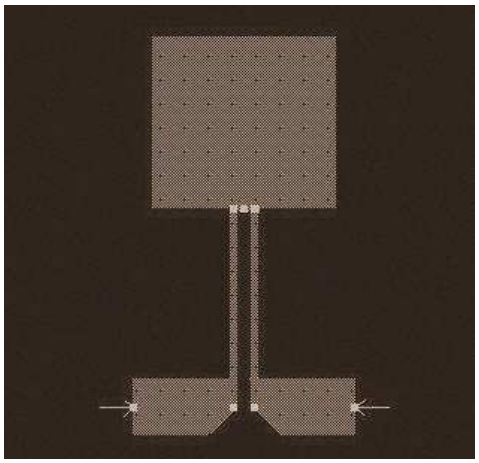

(a)

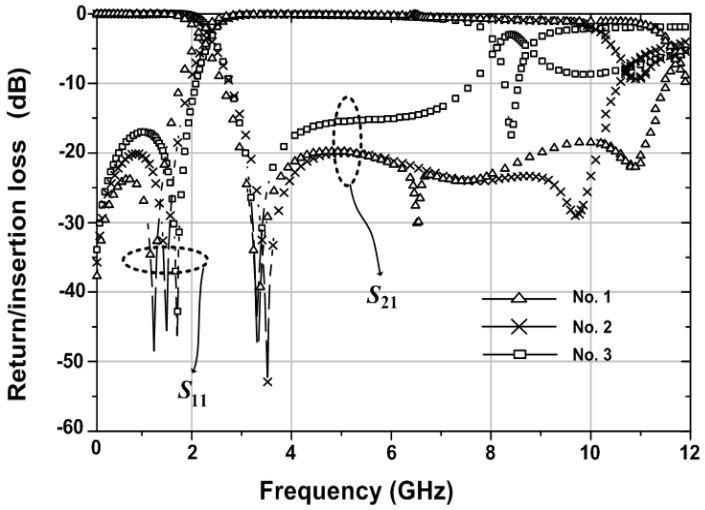

(b)

Fig. 2.18 (a) Layout in ADS momentum simulator (b) simulated results following the physical parameters in Table 2.2.

length. The layout and the simulated results by using the Agilent ADS momentum simulator are shown in Fig. 2.18.

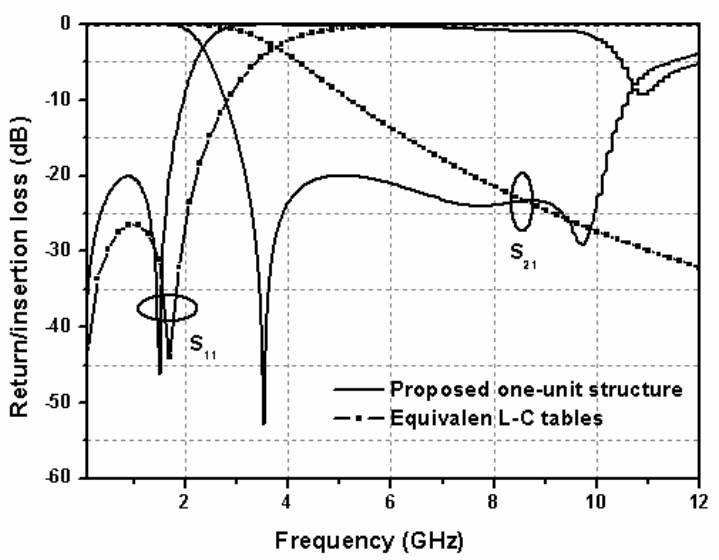

Fig. 2.19 Comparison between the two simulated results of the proposed one-unit structure and its equivalent *L-C* circuit.

Fig. 2.18 shows that the insertion loss within passband and the attenuation characteristics within stopband become better as the length of open-stub gets shorter. On the contrary, the circuit effective area is increased, as shown in Table II. We therefore adopted the 2nd set of dimensions to implement a compact low-pass filter. In this case, the simulated results show that the passband insertion loss is less than 0.3 dB over the whole passband, and the return loss is better than -20 dB from DC to -1.7 GHz, and the attenuation level is less than -20 dB within a very broad stopband up to about 10 GHz.

A comparison between the two simulated results of the proposed one-unit low-pass filter and its L-C equivalent circuit using the

lumped element values indicated in Fig. 2.17(b) has been made, as shown in Fig. 2.19. Viewing the comparison results, the proposed low-pass filter has very broad stopband as well as the prototype L-C low-pass filter, and has much sharper skirt characteristic but a little more insertion loss compared to the conventional L-C one.

Following the above analysis, a photograph of the fabricated 3rd Chebyshev low-pass prototype filter using the proposed one-unit structure is shown a compact microstrip low-pass filter has been fabricated based on a Taconic PCB with 0.35 thickness and relative dielectric constant of 1.524, as shown in Fig. 2.20, and the measured results are compared with the simulation study in Fig. 2.21. As is

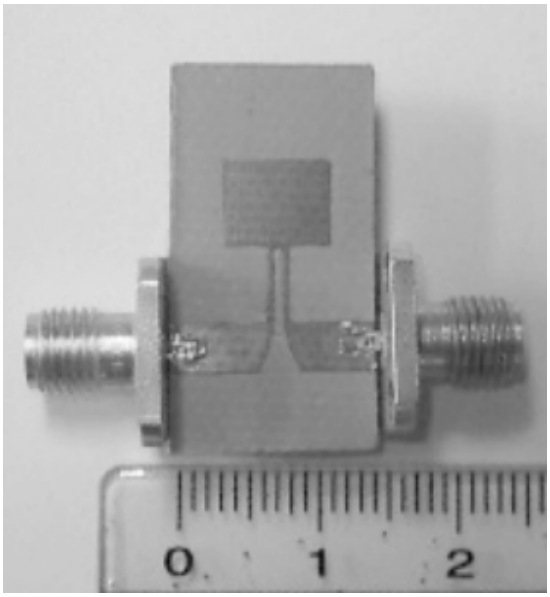

Fig. 2.20 A photograph of the fabricated compact microstrip low-pass filter.

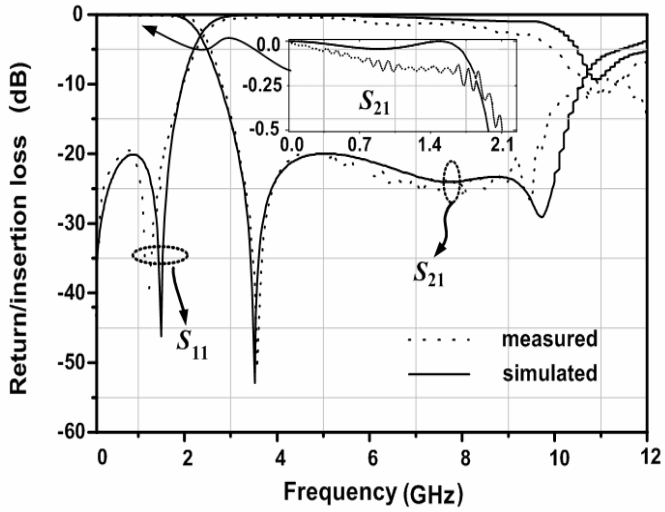

Fig. 2.21 Measured and simulated frequency responses.

depicted, the simulated results and the measured results agree well, obviously.

B. Low-pass filter using cascaded structure

In order to have a better skirt and stopband rejection characteristics, a low-pass filter using two cascaded stages are developed, the layout and lumped equivalent modeling are described in Fig. 2.22(a) and Fig. 2.22(b), respectively. Similar with the one-stage low-pass filter, a 5-order 0.01-dB ripple Chebyshev low-pass prototype filter with 3-dB cutoff frequency at 2 GHz are employed in this case, and the lumped elements values are indicated in Fig. 2.23. The physical dimensions of the two-stage low-pass filter can be obtained by the same method used in the one-stage case. However, the

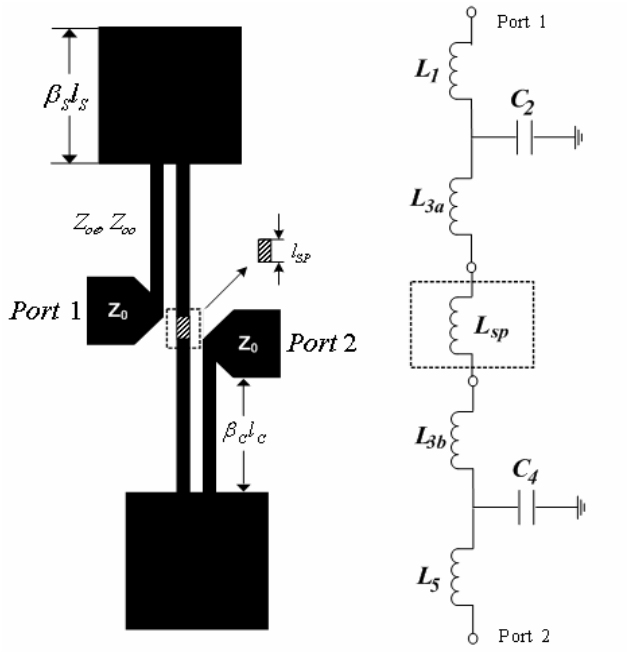

(a) (b)

Fig. 2.22 Low-pass filter using cascaded structure. (a) layout. (b) equivalent circuit.

lumped elements values of the 5-order Chebyshev prototype low-pass filter are not available, if the two stages are linked directly. Because the inductance values of L_1, L_2, L_{3a}, L_{3b}, and L_5 can be set to 3.009 nH as shown in Fig. 2.22(b), but a sum of the inductance values of L_{3a}, and L_{3b} is a litter less than the inductance value of L_3. Therefore, a short single transmission line with a length of l_{SP}, which can be modeled as a series inductor, is embedded between the two stages to meet the specific inductance value of L_3. Moreover, the width of the embedded transmission line is set to the same one as the symmetrical parallel coupled-line to avoid the transmission line discontinuity. The

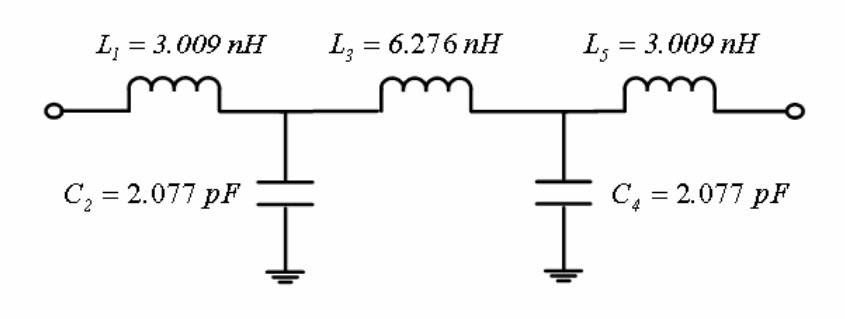

Fig. 2.23 5th Chebyshev prototype low-pass filter.

Table 2.3 Physical dimensions of the proposed two-stage low-pass filter

Parallel coupled-line (mm)			Open-stub (mm)		Embedded transmission line (mm)	
Width	Length	Space	Width	Length	Width	Length
0.65	7.60	0.65	6.8	6.8	0.65	0.5

length of l_{SP} is given by [28]

$$l_{SP} = \frac{\lambda_{gL}}{2\pi} sin^{-1}\left(\frac{\omega_C L_{SP}}{Z_{0L}}\right) \tag{2.12}$$

where λ_{gL} and Z_{OL} are the guided wavelength and characteristic impedance of the embedded transmission line, and ω_c is the angular cutoff frequency, L_{SP} is the inductance value of the equivalent series inductor.

$$L_{SP} = L_3 - L_{3a} - L_{3b} \tag{2.13}$$

where L_3 = 6.276 nH, L_{3a} = L_{3b} = 3.009 nH.

Table 2.3 shows the extracted physical dimensions of the proposed two-stage low-pass filter from the equivalent circuit, based on a 1.524 mm thickness Taconic PCB with a relative dielectric constant of 3.5. As shown in Fig. 2.24, a comparison is made between the dimensions of the proposed and conventional stepped-impedance low-pass filters. The proposed one is more compact on structure than the conventional one, and obviously, the large the order number of the prototype filter is, the more relatively compact and area-effective the proposed one becomes. The optimized simulation results of the proposed two-stage low-pass filter are shown in Fig. 2.24, and compared with those of the conventional stepped-impedance and

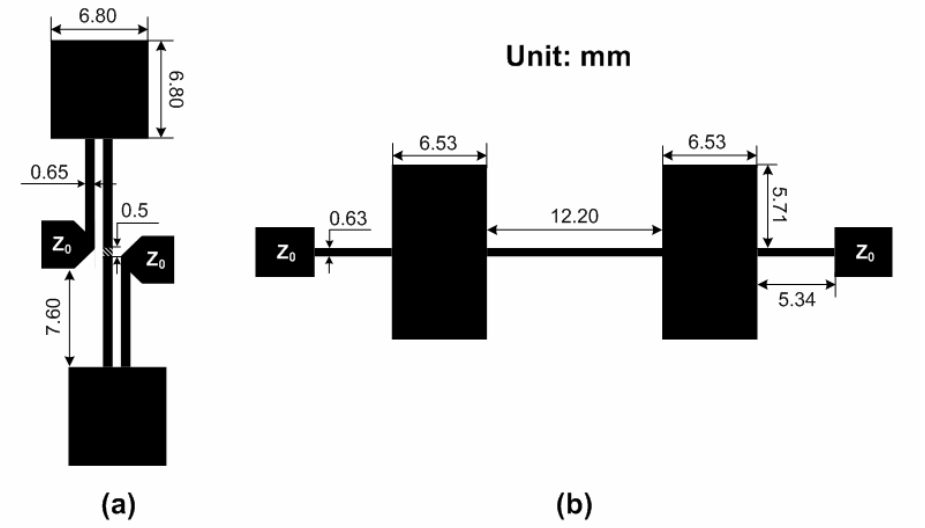

Fig. 2.24 Layouts of (a) the proposed two-stage and (b) conventional stepped-impedance low-pass filter.

equivalent *L-C* prototype low-pass filter. Inspecting the simulation results, the two-stage low-pass filter using the proposed structure provides a much sharper skirt characteristic and deeper rejection band compared to the results of the conventional one.

A photograph of the proposed two-stage low-pass filter is shown in Fig. 2.26. The measured frequency responses are shown in Fig. 2.27 in comparison with the simulated ones. As shown in Fig. 2.27, the measured and simulated results agree very well. This filter has a 3-dB cutoff frequency at 1.99 GHz. The return loss is greater than 20 dB from DC to 1.67 GHz. The insertion loss is less than 0.2 dB from DC to 1.6 GHz. The rejection is greater than 20 dB from 2.32 to 8.5 GHz.

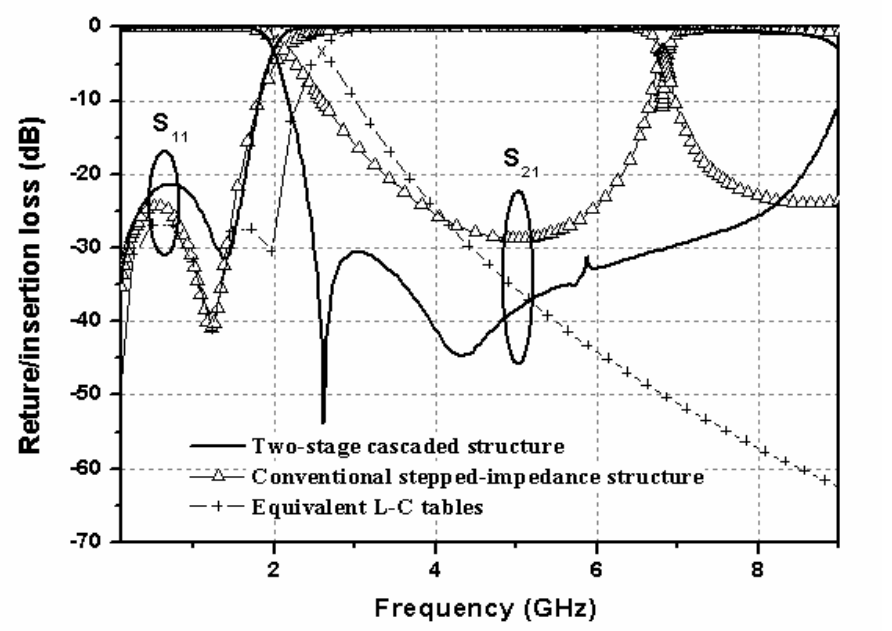

Fig. 2.25 Simulated frequency responses of the filter using equivalent *L-C* tables, conventional stepped-impedance and two-stage cascaded structure.

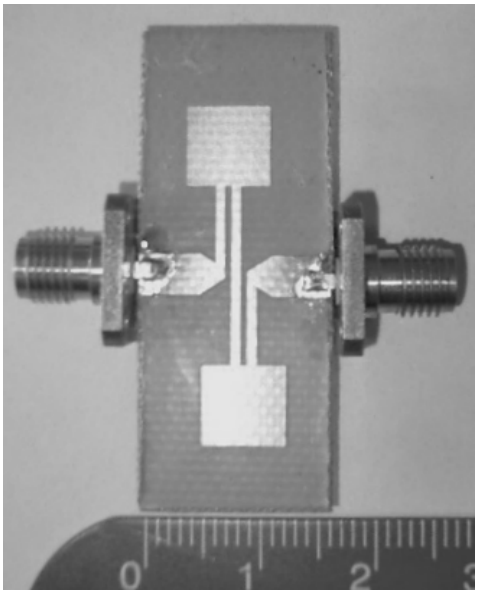

Fig. 2.26 Photograph of the proposed two-stage low-pass filter.

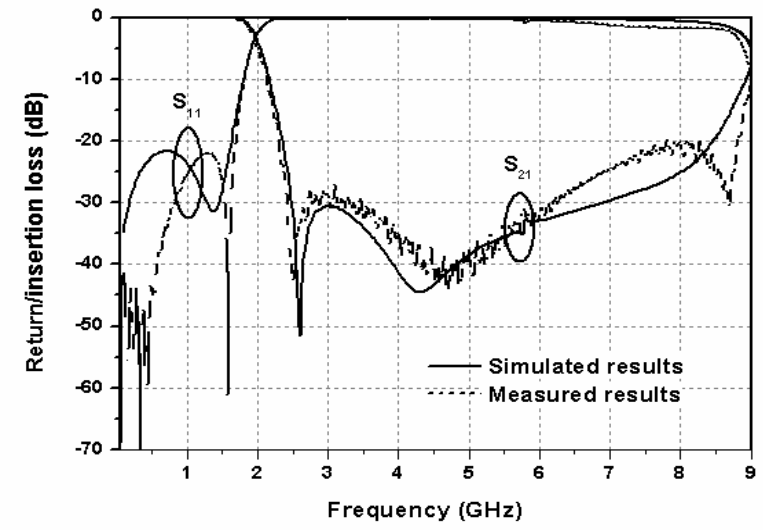

(a)

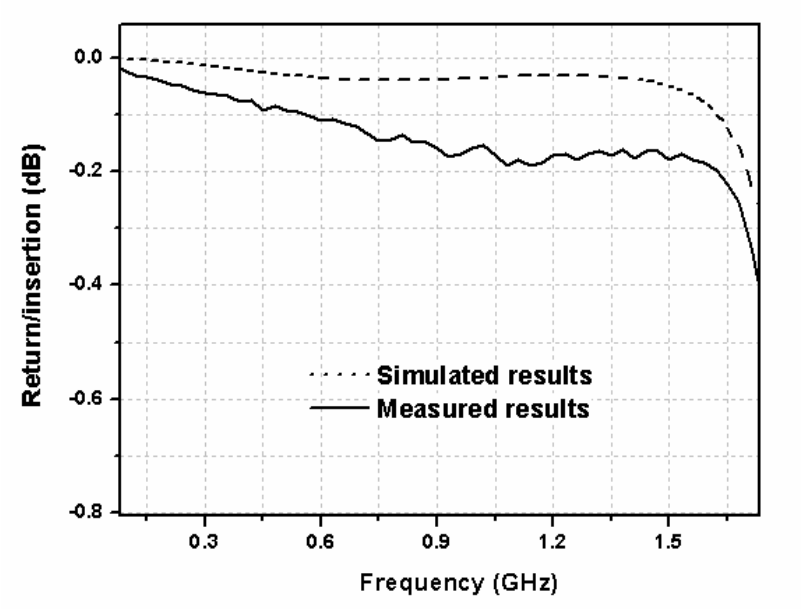

(b)

Fig. 2.27 Measured and simulated: (a) frequency responses and (b) S_{21} within the 3-dB bandwidth for the filter using the two-stage structure.

In this chapter, a new compact low-pass filter with very simple structure and its equivalent-circuit model have been developed in this paper. A 3- and a 5-order Chebyshev prototype low-pass filters have been synthesized from the equivalent-circuit using the published element-value tables to validate its correctness. Based on our observations on simulation performance and measurements, the new type of compact low-pass filter demonstrated many desirable features: low passband insertion loss, sharp skirt characteristic and broad stopband. Also, our design can be further extended and used in more high order design process to achieve more sharp skirt characteristic and deeper rejection band.

The low-pass filter proposed here is quite useful for applications in modern communication systems.

However, from the comparison results between the simulated results of the proposed low-pass filter based on microstrip line structure and its equivalent circuit based on Chebyshev prototype, we found that the proposed compact low-pass filter has the same cut-off frequency as the equivalent circuit, but the transmission-zero point cannot be represented by the equivalent circuit. Therefore, the equivalent circuit should be improved to descript the frequency responses of the proposed compact structure more exactly.

In next chapter, a modified equivalent circuit will be proposed.

CHAPTER 3 Equivalent Circuit Analysis

To develop a more exact equivalent circuit, we propose a new scheme in this chapter. Also, the proposed compact structure is divided into two parts, one is the parallel coupled-line with its far-end shorted and the other is the open-stub. However, the parallel coupled-line section is transformed into a different network topology as the one above-mentioned in chapter 2.

3.1 Equivalent circuit analysis

As shown in Fig. 3.1 below, the parallel coupled-line with its far-end shorted can be approximately modeled as transformer with one-end shorted.

Z_{oe} and Z_{oo} represent the even- and odd-mode impedance of the parallel coupled-line, respectively. θ is the electrical length of the coupled-line. L and M mean the self-inductance and mutual-inductance of the two identical inductors. C_c and C_g are two parasitic capacitors.

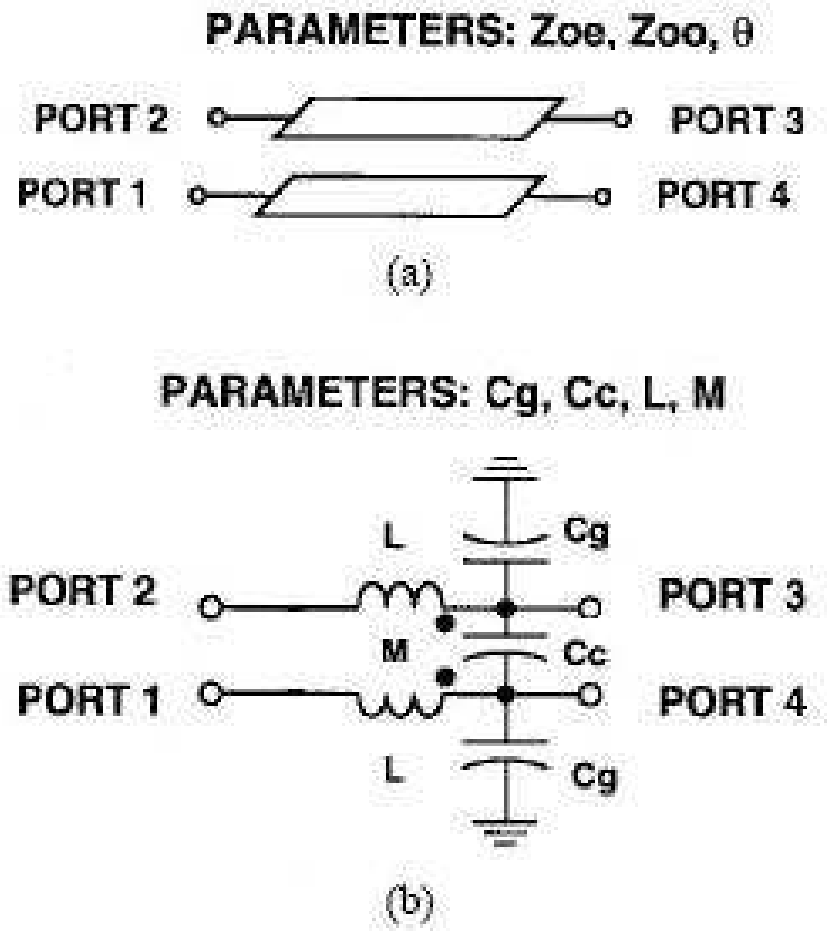

Fig. 3.1 (a) A parallel coupled-line section and (b) its corresponding equivalent circuit.

The values for L, M, C_c and C_g in terms of Z_{oe}, Z_{oo} and θ are as follows:

$$L = \frac{(Z_{oe} + Z_{oo})\sin\theta}{4\pi f} \tag{3.1}$$

$$M = \frac{(Z_{oe} - Z_{oo})\sin\theta}{4\pi f} \tag{3.2}$$

$$C_g = \frac{\tan(\theta/2)}{Z_{oe}\,2\pi f} \tag{3.3}$$

$$C_C = \left(\frac{1}{Z_{oo}} - \frac{1}{Z_{oe}}\right)\frac{\tan(\theta/2)}{4\pi f} \tag{3.4}$$

The values of the lumped element model are given in terms of coupled line parameters in a homogeneous medium. Once the lumped elements are determined, any structure which yields the correct lumped element values may be used, whether or not homogenous.

In this case, the parasitic capacitor C_C can be eliminated because the far-end of the parallel coupled-line is shorted. In addition, the other parasitic capacitor C_g can be omitted due to its very small value. Therefore, the parallel coupled-line with its far-end shorted will be approximately modeled as a transformer. And the open-stub is modeled as a capacitor as shown in Fig. 2.13. So far, the proposed compact structure can be modeled as shown in Fig. 3.2.

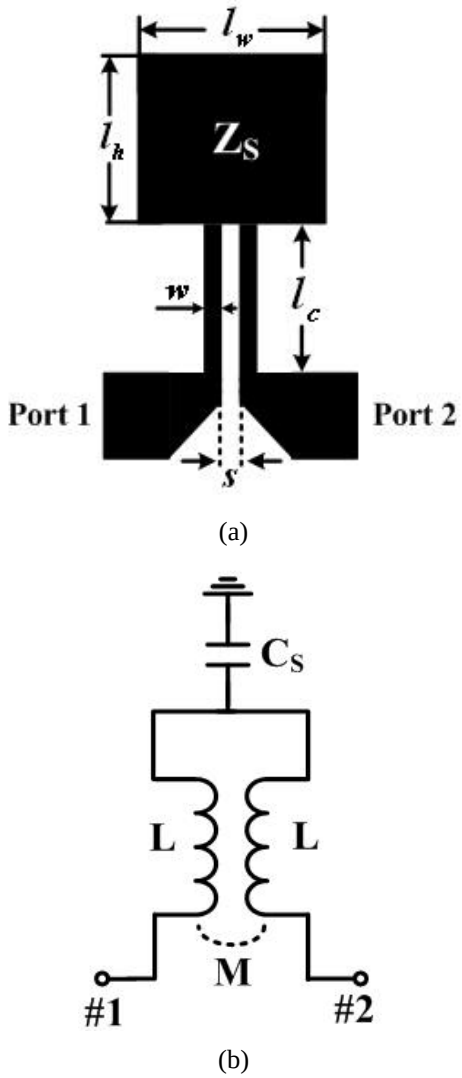

Fig. 3.2 (a) Layout of the proposed LPF and (b) general equivalent circuit.

Here, the present transformer can be father transformed into *pi*-type network without mutual-inductance, as depicted in Fig. 3.3.

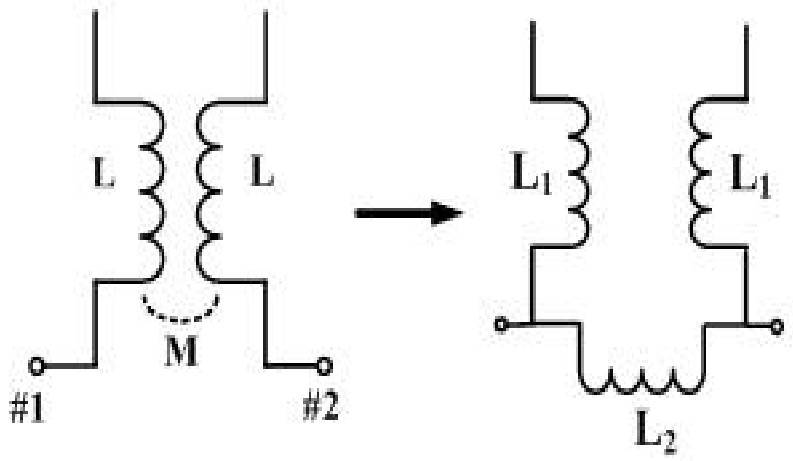

Fig. 3.3 Coupled-inductor model.

The relationship between the transformer and *pi*-type network can be obtained by the following equations [29], [30]:

$$L_1 = L + M \tag{3.5}$$

$$L_2 = \left(L^2 - M^2\right)/M \tag{3.6}$$

3.2 Discontinuity model

To obtain a more exact equivalent circuit, the discontinuity between the parallel coupled-line and the open-stub cannot be neglected. The discontinuity modeling is described in Fig. 3.4 and the element values can be calculated by Eqn. (3.7) ~ (3.11). [28],[32]

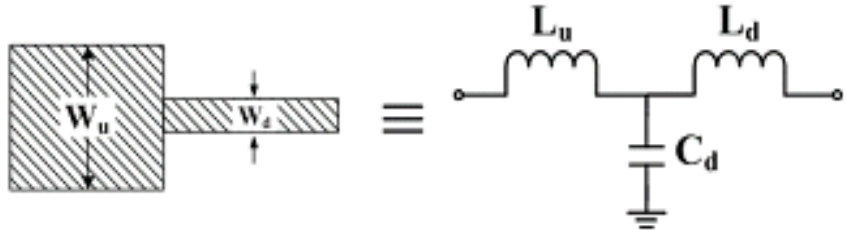

Fig. 3.4 Discontinuity model.

$$L_S = 0.000987\,h\left(1-\frac{Z_u}{Z_d}\right)^2 \tag{3.7}$$

$$C_d = 0.00137\,h\frac{\sqrt{\varepsilon_r}}{Z_u}\left(1-\frac{W_d}{W_u}\right)h\left[\frac{\sqrt{\varepsilon_r}+0.3}{\sqrt{\varepsilon_r}-0.258}\right]\cdot\left[\frac{W_u/h+0.264}{W_d/h+0.8}\right] \tag{3.8}$$

$$L_u = \frac{Z_u\sqrt{\varepsilon_r}}{c}L_s \tag{3.9}$$

$$L_d = \frac{Z_d\sqrt{\varepsilon_r}}{c}L_s \tag{3.10}$$

where h and ε_r represent the thickness and the relative dielectric constant of the microstrip substrate, respectively. c is the velocity of the light, W_u and W_d represent the widths of the corresponding transmission lines as shown in Fig. 3.4.

Therefore, the final equivalent circuit is shown in Fig. 3.5 below.

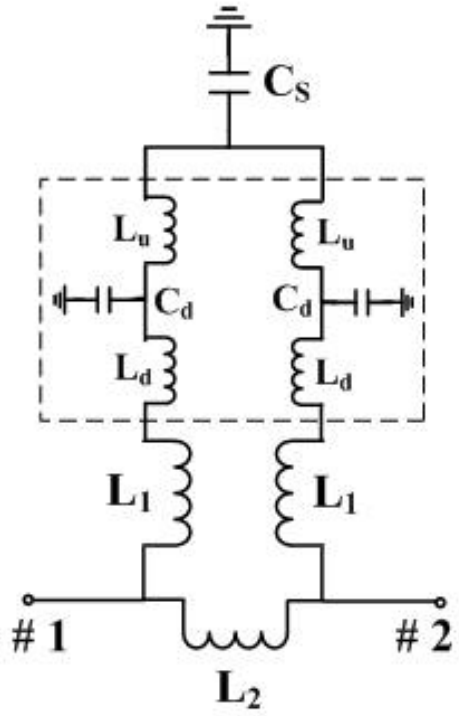

Fig. 3.5 Proposed equivalent circuit.

Table 3.1 Proposed compact low-pass filter

	Parameters	
Open-stub	Width	7.10 mm
	Length	6.00 mm
Coupled line	Width	0.36 mm
	Length	5.50 mm
	Space	0.67 mm
ε_r= 3.5, Substrate thickness: 1.524 mm		

Table 3.2 Equivalent circuit

	Parameters
L_1	4.70 nH
L_2	9.30 nH
L_d	0.72 nH
L_u	0.17 nH
C_d	0.13 pF
C_s	1.20 pF

The physical dimensions of the designed compact low-pass filter are shown in Table one, where the relative dielectric constant is 3.5, and the substrate thickness is 1.524 mm. Based on the before-mentioned formulas, the lumped elements values of its equivalent circuit are calculated and shown in Table 3.1 and 3.2.

To examine the validity of the equivalent circuit, a comparison of simulated results between the proposed microstrip structure and its equivalent circuit was made. From figure 3.6, we can find that the simulated results of the proposed low-pass filter described as the circle-marked line and the simulated results of its equivalent circuit described as the solid-line agree very well. And then compared with the conventional stepped-impedance low-pass filter, the proposed one has broad rejection bandwidth and sharp skirt characteristics due to a

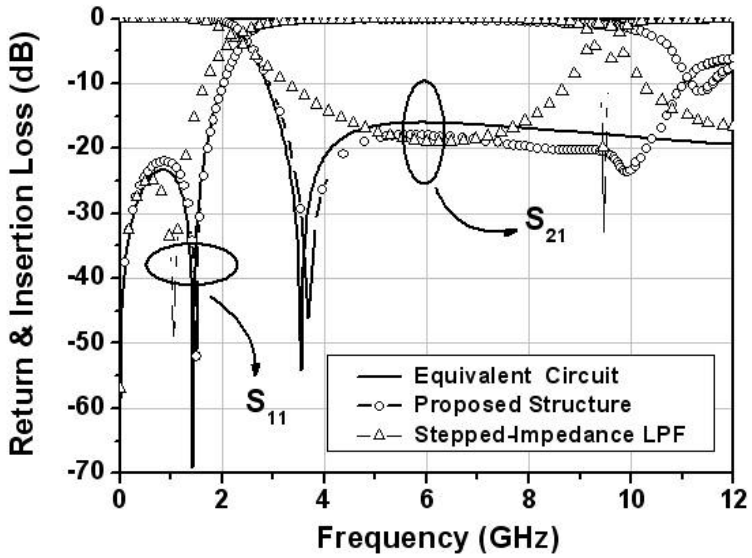

Fig. 3.6 Comparison between the two simulated results of the proposed structure and its equivalent circuit.

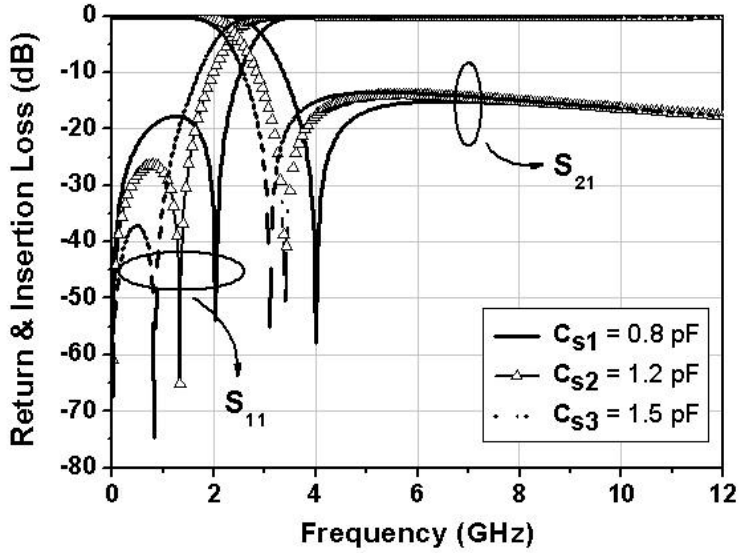

(a)

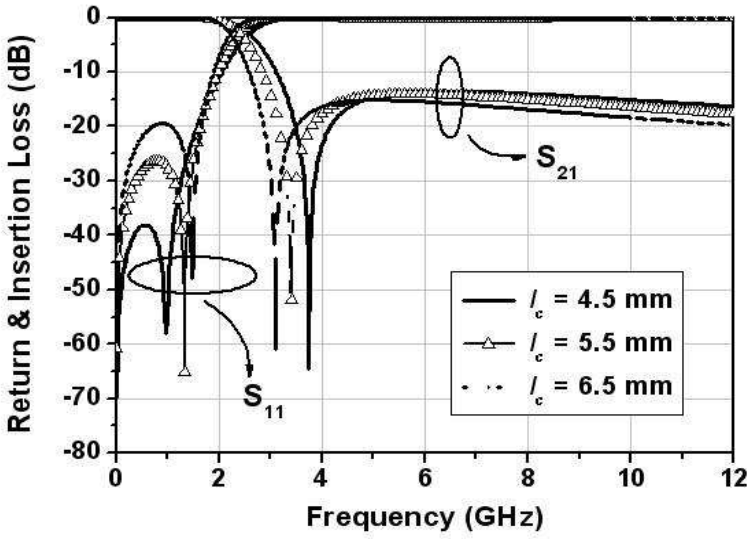

(b)

Fig. 3.7 Low-pass filters with (a) different open-stop length, namely, with different C_s , (b) different length.

finite attenuation pole near to the cut-off frequency. Moreover, the

proposed low-pass filter has low insertion loss at passband.

To find an optimal frequency response for this type of low-pass filter, we have performed two tests for the tuning of finite attenuation pole. One is by changing the open-stub length based on the same dimensions of the parallel coupled line. The other is by changing the coupled-line length without changing the open-stub's dimensions. As shown in Fig. 3.7(a), we can observe that the finite attenuation pole shifts to the upper frequency as the shunted capacitor value decreases, at the same time, the insertion loss increases. And as shown in Fig. 3.7(b), the finite attenuation pole shifts to the higher frequency as the coupled-line length decreases, and simultaneously, the insertion loss decreases.

In order to validate the proposed design approach, a microstrip low-pass filter under C_s = 1.20 *pF* is fabricated based on a 1.524 mm thickness Taconic substrate with relative dielectric constants of ε_r= 3.5. The low-pass filter is measured with Anritsu 37369D network analyzer. A photograph of the fabricated filter is shown in Fig. 3.8, and the measured results are compared with the simulation study for C_s = 1.20 *pF*. As shown in Fig. 3.9, the measured and simulated results agree very well. A finite attenuation pole appears at 3.5 GHz up to 53 dB to improve selectivity characteristic of low-pass filter. The return loss within passband is less than -20 dB from DC to 1.8 GHz. The insertion loss is very low and it is almost less than 0.25 dB from DC to 1.75 GHz. The rejection level within stopband is greater than 20 dB from 3.1 to 9.5 GHz, which is a very broad rejection band.

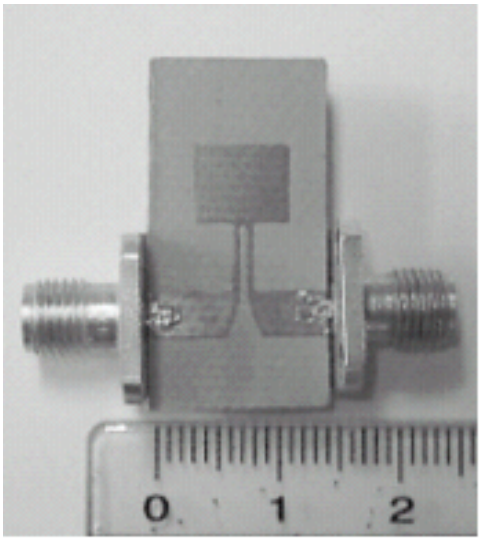

Fig. 3.8 A photograph of the fabricated low-pass filter.

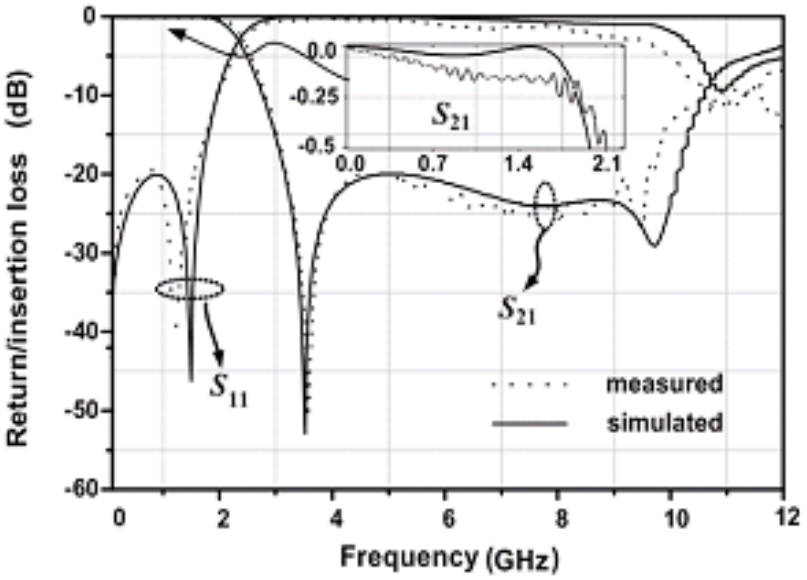

Fig. 3.9 Measured and simulated frequency responses.

From the above analysis, the equivalent circuit proposed in this chapter has more exact performances as the compact microstrip structure; particularly the first transmission zero in frequency domain can be controllable by adjusting the physical parameters.

As is well know, it is very convenient that an appropriate equivalent circuit can be employed to design a distributed circuit. However, the equivalent circuit comprised of the lumped elements has their limitations in frequency responses. Because the microwave circuits made of the distributed elements have some kind of periodic frequency responses which can not be described exactly. Therefore, the frequency responses should be validated based on distributed transmission line-model; these will be discussed in next chapter.

CHAPTER 4 Transmission-Line Model

In this chapter, the proposed compact structure will be analyzed based on a transmission-line model using even-odd mode analysis method and basic two-port network theory. A detail analysis process is introduced step-by-step.

4.1 Review of two-port network theory

A. Definition of two-port network and its network parameters

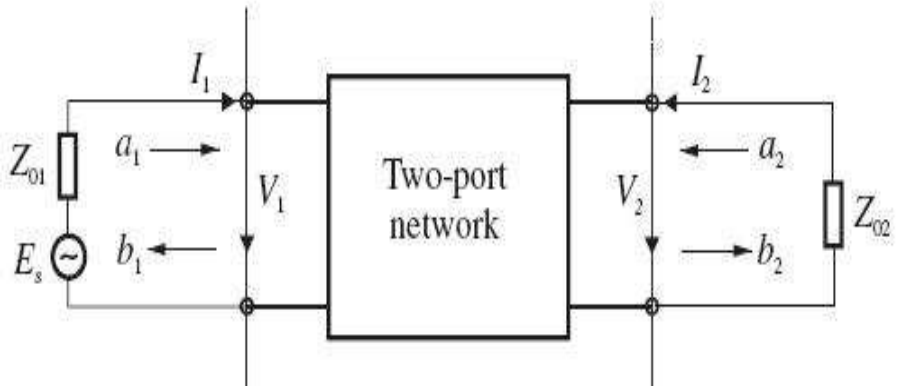

Fig. 4.1 General Two-port network [*S*].

Most RF/microwave filters and filter components can be represented by a two-port network, as shown in Figure 4.1, where V_1,

V_2 and I_1, I_2 are the voltage and current variables at the ports 1 and 2, respectively, Z_{01} and Z_{02} are the terminal impedances, and Es is the source or generator voltage. Note that the voltage and current variables are complex amplitudes when we consider sinusoidal quantities.

Because it is difficult to measure the voltage and current at microwave frequencies, the wave variables a_1, b_1 and a_2, b_2 are introduced, with a indicating the incident waves and b the reflected waves. The relationships between the wave variables and the voltage and current variables are defined as:

$$\boldsymbol{V_n = \sqrt{Z_{on}}\left(a_n + b_n\right)} \tag{4.1}$$

$$\boldsymbol{I_n = \frac{1}{\sqrt{Z_{on}}}\left(a_n - b_n\right)} \tag{4.2}$$

or

$$\boldsymbol{a_n = \frac{1}{2}\left(\frac{V_n}{\sqrt{Z_{on}}} + \sqrt{Z_{on}} I_n\right)} \tag{4.3}$$

$$\boldsymbol{b_n = \frac{1}{2}\left(\frac{V_n}{\sqrt{Z_{on}}} - \sqrt{Z_{on}} I_n\right)} \tag{4.4}$$

・*Impedance parameters*

Impedance or *Z* parameters of a two-port network are defined as

$$\boldsymbol{Z}_{11} = \left.\frac{\boldsymbol{V}_1}{\boldsymbol{I}_1}\right|_{\boldsymbol{I}_2=0}, \qquad \boldsymbol{Z}_{12} = \left.\frac{\boldsymbol{V}_1}{\boldsymbol{I}_2}\right|_{\boldsymbol{I}_1=0}$$

$$\boldsymbol{Z}_{21} = \left.\frac{\boldsymbol{V}_2}{\boldsymbol{I}_1}\right|_{\boldsymbol{I}_2=0}, \qquad \boldsymbol{Z}_{22} = \left.\frac{\boldsymbol{V}_2}{\boldsymbol{I}_2}\right|_{\boldsymbol{I}_1=0} \tag{4.5}$$

where $I_n = 0$ implies a perfect open-circuit at port *n*. These definitions can be written as

$$\begin{bmatrix}\boldsymbol{V}_1\\ \boldsymbol{V}_2\end{bmatrix} = \begin{bmatrix}\boldsymbol{Z}_{11} & \boldsymbol{Z}_{12}\\ \boldsymbol{Z}_{21} & \boldsymbol{Z}_{22}\end{bmatrix} \cdot \begin{bmatrix}\boldsymbol{I}_1\\ \boldsymbol{I}_2\end{bmatrix} \tag{4.6}$$

The matrix, which contains the *Z*-parameters, is denoted by [*Z*]. For reciprocal networks, $Z_{12} = Z_{21}$. If networks are symmetrical, $Z_{11} = Z_{22}$ and $Z_{12} = Z_{21}$. For a lossless network, the *Z* parameters are all purely imaginary.

· *Admittance parameters*

Admittance or *Y* parameters of a two-port network are defined as

$$\boldsymbol{Y}_{11} = \left.\frac{\boldsymbol{I}_1}{\boldsymbol{V}_1}\right|_{\boldsymbol{V}_2=0}, \qquad \boldsymbol{Y}_{12} = \left.\frac{\boldsymbol{I}_1}{\boldsymbol{V}_2}\right|_{\boldsymbol{V}_1=0}$$

$$\boldsymbol{Y}_{21} = \left.\frac{\boldsymbol{I}_2}{\boldsymbol{V}_1}\right|_{\boldsymbol{V}_2=0}, \qquad \boldsymbol{Y}_{22} = \left.\frac{\boldsymbol{I}_2}{\boldsymbol{V}_2}\right|_{\boldsymbol{V}_1=0} \tag{4.7}$$

where $V_n = 0$ implies a perfect short-circuit at port n. The definitions of the Y parameters may also be written as

$$\begin{bmatrix} \boldsymbol{I}_1 \\ \boldsymbol{I}_2 \end{bmatrix} = \begin{bmatrix} \boldsymbol{Y}_{11} & \boldsymbol{Y}_{12} \\ \boldsymbol{Y}_{21} & \boldsymbol{Y}_{22} \end{bmatrix} \cdot \begin{bmatrix} \boldsymbol{V}_1 \\ \boldsymbol{V}_2 \end{bmatrix} \tag{4.8}$$

where the matrix containing the Y-parameters, is denoted by [Y]. For reciprocal networks, $Y_{12} = Y_{21}$. If networks are symmetrical, $Y_{11} = Y_{22}$ and $Y_{12} = Y_{21}$. For a lossless network, the Y parameters are all purely imaginary.

· *ABCD parameters*

The *ABCD* parameters of a two-port network are given by

$$\boldsymbol{A} = \left.\frac{\boldsymbol{V}_1}{\boldsymbol{V}_2}\right|_{\boldsymbol{I}_2=0}, \qquad \boldsymbol{B} = \left.\frac{\boldsymbol{V}_1}{-\boldsymbol{I}_2}\right|_{\boldsymbol{V}_2=0}$$

$$\boldsymbol{C} = \left.\frac{\boldsymbol{I}_1}{\boldsymbol{V}_2}\right|_{\boldsymbol{I}_2=0}, \qquad \boldsymbol{D} = \left.\frac{\boldsymbol{I}_1}{-\boldsymbol{I}_2}\right|_{\boldsymbol{V}_2=0} \tag{4.9}$$

These parameters are actually defined in a set of linear equations in matrix notation

$$\begin{bmatrix}\boldsymbol{V}_1\\ \boldsymbol{I}_1\end{bmatrix} = \begin{bmatrix}\boldsymbol{A} & \boldsymbol{B}\\ \boldsymbol{C} & \boldsymbol{D}\end{bmatrix} \cdot \begin{bmatrix}\boldsymbol{V}_2\\ -\boldsymbol{I}_2\end{bmatrix} \tag{4.10}$$

where the matrix comprised of the *ABCD* parameters is called the *ABCD* matrix. Sometimes, it may also be referred to as the transfer or chain matrix. The *ABCD* parameters have the following properties:

$AD\text{-}BC = 1$ for a reciprocal network (4.11)

$A = D$ for a symmetrical network (4.12)

If the network is lossless, then *A* and *D* will be purely real and *B* and *C* will be purely imaginary.

The *ABCD* parameters are very useful for analysis of a complex two-port network that may be divided into two or more cascaded sub-networks.

- *Scattering parameters*

The scattering or *S* parameters of a two-port network are defined

in terms of the wave variables as

$$\boldsymbol{S}_{11} = \left.\frac{\boldsymbol{b}_1}{\boldsymbol{a}_1}\right|_{\boldsymbol{a}_2=0}, \qquad \boldsymbol{S}_{12} = \left.\frac{\boldsymbol{b}_1}{\boldsymbol{a}_2}\right|_{\boldsymbol{a}_1=0}$$

$$\boldsymbol{S}_{21} = \left.\frac{\boldsymbol{b}_2}{\boldsymbol{a}_1}\right|_{\boldsymbol{a}_2=0}, \qquad \boldsymbol{S}_{22} = \left.\frac{\boldsymbol{b}_2}{\boldsymbol{a}_2}\right|_{\boldsymbol{a}_1=0} \tag{4.13}$$

where $a_n = 0$ implies a perfect impedance match (no reflection from terminal impedance) at port n. These definitions may be written as

$$\begin{bmatrix}\boldsymbol{b}_1\\ \boldsymbol{b}_2\end{bmatrix} = \begin{bmatrix}\boldsymbol{S}_{11} & \boldsymbol{S}_{12}\\ \boldsymbol{S}_{21} & \boldsymbol{S}_{22}\end{bmatrix} \cdot \begin{bmatrix}\boldsymbol{a}_1\\ \boldsymbol{a}_2\end{bmatrix} \tag{4.14}$$

where the matrix containing the S parameters is referred to as the scattering matrix or S matrix, which may simply be denoted by [S].

The parameters S_{11} and S_{22} are also called the reflection coefficients, S_{12} and S_{21} the transmission coefficients. These are the parameters directly measurable at microwave frequencies. The S parameters are in general complex, and it is convenient to express them in terms of amplitudes and phases, i.e., $S_{mn} = |S_{mn}|e^{j\Phi mn}$ for m, n = 1,2. Often their amplitudes are given in decibels (dB), which are defined as

$$20\log|\boldsymbol{S}_{mn}|\,\boldsymbol{dB} \qquad \boldsymbol{m},\boldsymbol{n}=1,2 \tag{4.15}$$

where the logarithm operation is base 10. This will be assumed through this book unless otherwise stated. For filter characterization, we may define two parameters:

$$\boldsymbol{L_A} = -20\log|\boldsymbol{S}_{mn}|\,\boldsymbol{dB} \qquad \boldsymbol{m},\boldsymbol{n}=1,2(\boldsymbol{m}\neq\boldsymbol{n})$$

$$\boldsymbol{L_R} = 20\log|\boldsymbol{S}_{nn}|\,\boldsymbol{dB} \qquad \boldsymbol{n}=1,2 \tag{4.16}$$

where L_A denotes the insertion loss between ports n and m and L_R represents the return loss at port n. Instead of using the return loss, voltage standing wave ratio *VSWR* maybe used of *VSWR* is

$$\boldsymbol{VSWR} = \frac{1+|\boldsymbol{S}_{nn}|}{1-|\boldsymbol{S}_{nn}|} \qquad \boldsymbol{n}=1,2 \tag{4.17}$$

B. Network connections

Often in the analysis of a filter network, it is convenient to treat one or more filter components or elements as individual sub-networks, and then connect them to determine the network parameters of the filter. The three basic types of connection that are usually encountered are:

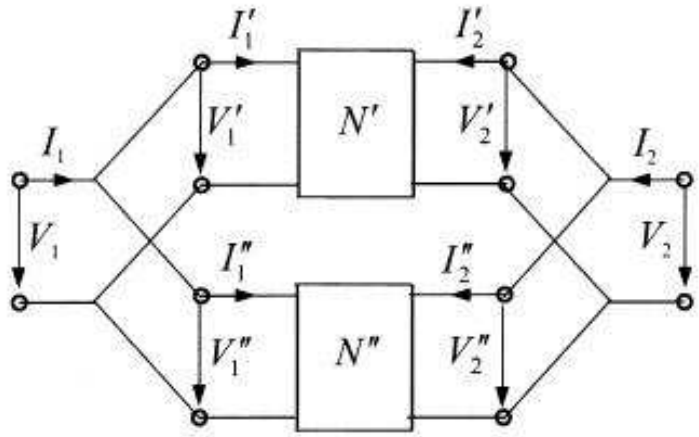

(a)

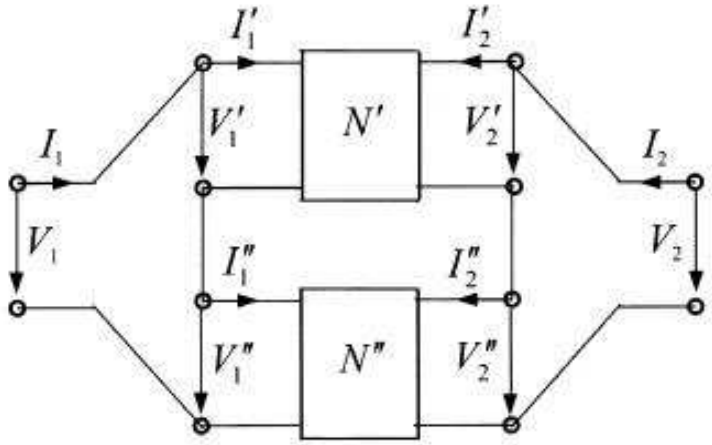

(b)

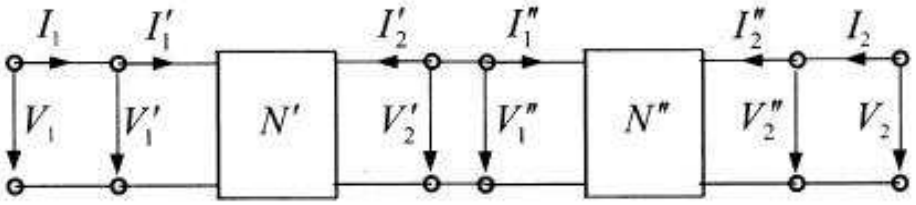

(c)

Fig. 4.2 Basic types of network connection: (a) parallel, (b) series, and (c) cascade.

1. Parallel

2. Series

3. Cascade

Suppose we wish to connect two networks N and N in parallel, as shown in Figure 4.2(*a*). An easy way to do this type of connection is to use their *Y* matrices. This is because

$$\begin{bmatrix} \boldsymbol{I}_1 \\ \boldsymbol{I}_2 \end{bmatrix} = \begin{bmatrix} \boldsymbol{I}_1^{'} \\ \boldsymbol{I}_2^{'} \end{bmatrix} + \begin{bmatrix} \boldsymbol{I}_1^{''} \\ \boldsymbol{I}_2^{''} \end{bmatrix} \quad \textbf{\textit{and}} \quad \begin{bmatrix} \boldsymbol{V}_1 \\ \boldsymbol{V}_2 \end{bmatrix} = \begin{bmatrix} \boldsymbol{V}_1^{'} \\ \boldsymbol{V}_2^{'} \end{bmatrix} + \begin{bmatrix} \boldsymbol{V}_1^{''} \\ \boldsymbol{V}_2^{''} \end{bmatrix}$$

Therefore,

$$\begin{bmatrix} \boldsymbol{I}_1 \\ \boldsymbol{I}_2 \end{bmatrix} = \left(\begin{bmatrix} \boldsymbol{Y}_{11}^{'} & \boldsymbol{Y}_{21}^{'} \\ \boldsymbol{Y}_{21}^{'} & \boldsymbol{Y}_{22}^{'} \end{bmatrix} + \begin{bmatrix} \boldsymbol{Y}_{11}^{''} & \boldsymbol{Y}_{21}^{''} \\ \boldsymbol{Y}_{21}^{''} & \boldsymbol{Y}_{22}^{''} \end{bmatrix} \right) \cdot \begin{bmatrix} \boldsymbol{V}_1 \\ \boldsymbol{V}_2 \end{bmatrix} \qquad (4.18)$$

or the *Y* matrix of the combined network is:

$$[\boldsymbol{Y}] = [\boldsymbol{Y}^{'}] + [\boldsymbol{Y}^{''}] \qquad (4.19)$$

This type of connection can be extended to more than two two-port networks connected in parallel. In that case, the short-circuit admittance matrix of the composite network is given simply by the sum of the short-circuit admittance matrices of the individual networks.

Analogously, the networks of Figure 4.2(*b*) are connected in

series at both their input and output terminals; consequently

$$\begin{bmatrix} V_1 \\ V_2 \end{bmatrix} = \begin{bmatrix} V_1' \\ V_2' \end{bmatrix} + \begin{bmatrix} V_1'' \\ V_2'' \end{bmatrix} \quad \textit{and} \quad \begin{bmatrix} I_1 \\ I_2 \end{bmatrix} = \begin{bmatrix} I_1' \\ I_2' \end{bmatrix} + \begin{bmatrix} I_1'' \\ I_2'' \end{bmatrix}$$

This gives

$$\begin{bmatrix} V_1 \\ V_2 \end{bmatrix} = \left(\begin{bmatrix} Z_{11}' & Z_{21}' \\ Z_{21}' & Z_{22}' \end{bmatrix} + \begin{bmatrix} Z_{11}'' & Z_{21}'' \\ Z_{21}'' & Z_{22}'' \end{bmatrix} \right) \cdot \begin{bmatrix} I_1 \\ I_2 \end{bmatrix} \qquad (4.20)$$

and thus the resultant *Z* matrix of the composite network is given by

$$[Z] = [Z'] + [Z''] \qquad (4.21)$$

Similarly, if there are more than two two-port networks to be connected in series to form a composite network, the open-circuit impedance matrix of the composite network is equal to the sum of the individual open-circuit impedance matrices.

The cascade connection of two or more simpler networks appears to be used most frequently in analysis and design of filters. This is because most filters consist of cascaded two-port components. For simplicity, consider a network formed by the cascade connection of two sub-networks, as shown in Figure 4.2(c). The following terminal voltage and current relationships at the terminals of the composite network would be obvious:

$$\begin{bmatrix} V_1 \\ I_1 \end{bmatrix} = \begin{bmatrix} V_1^{'} \\ I_1^{'} \end{bmatrix} \quad \textit{and} \quad \begin{bmatrix} V_2 \\ I_2 \end{bmatrix} = \begin{bmatrix} V_2^{''} \\ I_2^{''} \end{bmatrix}$$

It should be noted that the outputs of the first sub-network $N^{'}$ are the inputs of the following second sub-network $N^{''}$, namely

$$\begin{bmatrix} V_2 \\ -I_2^{'} \end{bmatrix} = \begin{bmatrix} V_1^{''} \\ I_1^{''} \end{bmatrix}$$

If the networks $N^{'}$ and $N^{''}$ are described by the *ABCD* parameters, these terminal voltage and current relationships all together lead to

$$\begin{bmatrix} V_1 \\ I_1 \end{bmatrix} = \left(\begin{bmatrix} A^{'} & B^{'} \\ C^{'} & D^{'} \end{bmatrix} \cdot \begin{bmatrix} A^{''} & B^{''} \\ C^{''} & D^{''} \end{bmatrix} \right) \cdot \begin{bmatrix} V_2 \\ -I_2 \end{bmatrix} = \begin{bmatrix} A & B \\ C & D \end{bmatrix} \cdot \begin{bmatrix} V_2 \\ -I_2 \end{bmatrix} \quad (4.22)$$

Thus, the transfer matrix of the composite network is equal to the matrix product of the transfer matrices of the cascaded sub-networks. This argument is valid for any number of two-port networks in cascade connection.

4.2 Transmission line modeling

As discussed in chapter 1 and chapter 2, two kinds of equivalent circuits have been proposed. It is very convenient that the equivalent circuit is extracted. However, due to some limitations of the equivalent circuit comprised of the lumped-elements, the exact

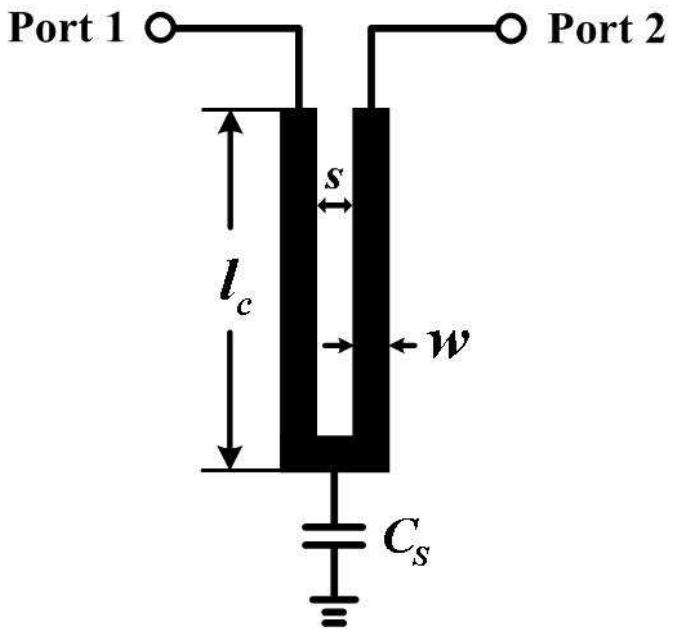

Fig. 4.3 Transmission line model.

frequency characterizations cannot be described completely. Therefore, the frequency responses based on transmission line-modeling have to be investigated. In this section, the detail investigation process is introduced next.

As shown in Fig. 4.3, the transmission line model is almost the same as the proposed compact structure. However, the circuit is analyzed by using the basic two-port network theory and even-odd mode method.

As depicted in Fig. 4.4(a), the total *Z*-matrix of a serially connected network can be given by the equation below:

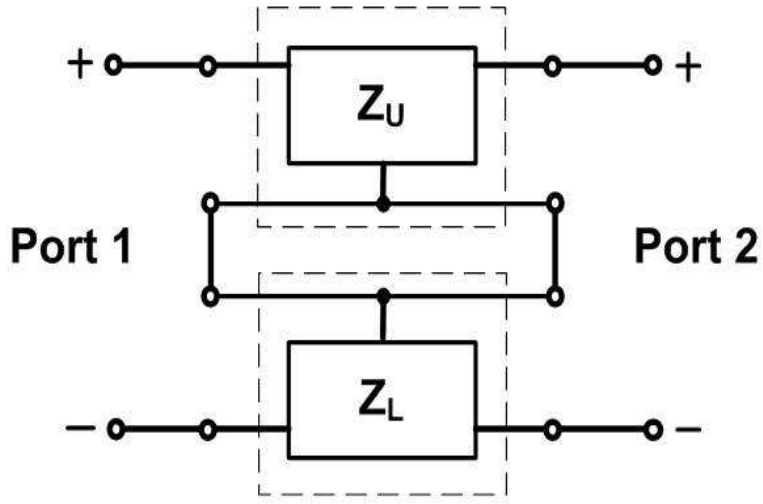

(a)

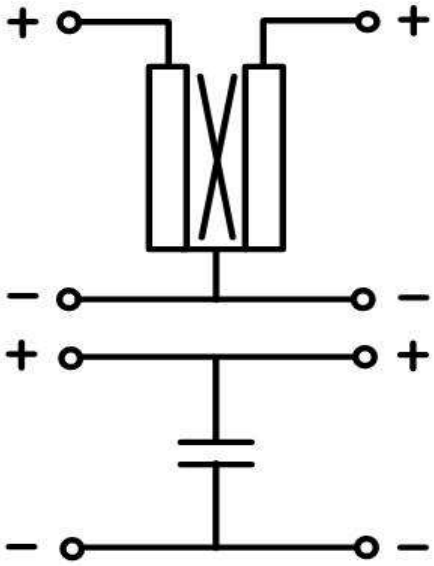

(b)

Fig. 4.4 (a) Serially connected two-port network. (b) Decomposition diagram of the proposed structure.

$$[Z_T] = [Z_U] + [Z_L] \tag{4.23}$$

where $[Z_T]$ is the total *Z*-parameters, $[Z_U]$ is the *Z*-parameters of the upper sub-network, and $[Z_L]$ is the *Z*-parameters of the lower sub-network, respectively.

Referred to Fig. 4.4(b), the parallel coupled-line and the capacitive load sections can be seen as the upper and lower networks, respectively. For the upper network, the elements of the impedance matrix $[Z_U]$ can be calculated by using even-odd mode analysis method.

A Upper sub-network (coupled-line)

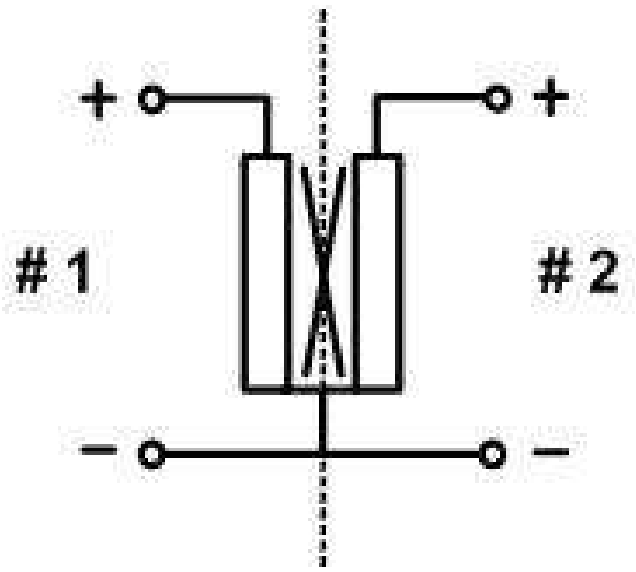

Fig. 4.5 Upper sub-network

$$\boldsymbol{Z}_{11}^{U} = \boldsymbol{j}\left(\boldsymbol{Z}_{oe}\tan\boldsymbol{\theta}_{e} + \boldsymbol{Z}_{oo}\tan\boldsymbol{\theta}_{o}\right)/2 \tag{4.24}$$

$$\boldsymbol{Z}_{21}^{U} = \boldsymbol{j}\left(\boldsymbol{Z}_{oe}\tan\boldsymbol{\theta}_{e} - \boldsymbol{Z}_{oo}\tan\boldsymbol{\theta}_{o}\right)/2 \tag{4.25}$$

As indicated in Eqn. (4.24) and (4.25), $\boldsymbol{Z}_{11}^{U}$ is the sum of $\boldsymbol{Z}_{in}^{e}/2$ and $\boldsymbol{Z}_{in}^{o}/2$, and $\boldsymbol{Z}_{21}^{U}$ is the difference of $\boldsymbol{Z}_{in}^{e}/2$ and $\boldsymbol{Z}_{in}^{o}/2$. θ_e, θ_o represent the even- and odd mode electrical length, respectively.

B Lower sub-network (load capacitor)

For the lower network, the elements in $[Z_L]$ are all the same and can be derived as:

$$\boldsymbol{Z}_{mn} = -\boldsymbol{j}/\left(\boldsymbol{\omega C}_{S}\right), \quad \boldsymbol{m},\boldsymbol{n} = 1, 2. \tag{4.26}$$

From the relationship between the impedance and scattering matrices, the transmission parameter of the network can be obtained by [24]

$$\boldsymbol{S}_{21} = \frac{2\boldsymbol{Z}_{12}^{T}\boldsymbol{Z}_{0}}{(\boldsymbol{Z}_{11}^{T} + \boldsymbol{Z}_{0})(\boldsymbol{Z}_{22}^{T} + \boldsymbol{Z}_{0}) - \boldsymbol{Z}_{12}^{T}\boldsymbol{Z}_{21}^{T}} \tag{4.27}$$

where Z_0 is the input and output microstrip line characteristic impedance. The finite attenuation poles are located at the angular frequencies ω where $S_{21}(\omega) = 0$ or $Z_{21}(\omega) = 0$. Therefore, the frequencies of the finite attenuation poles should satisfy the following

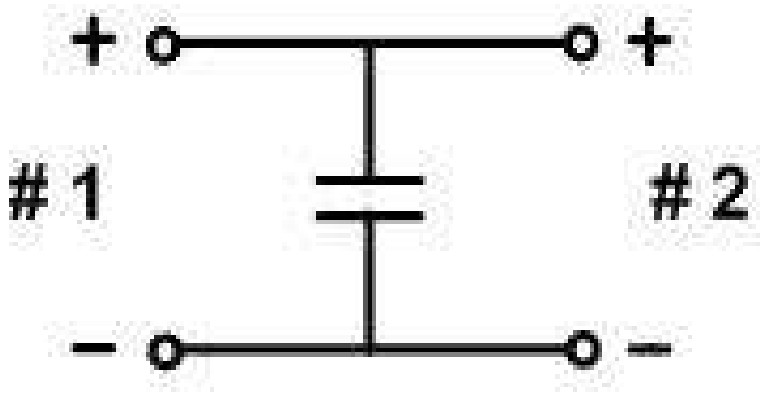

Fig. 4.6 Lower sub-network

equation derived from (4.25) and (4.26):

$$\left(Z_{oe}\tan\theta_e - Z_{oo}\tan\theta_o\right)/2 = 1/\left(\omega C_S\right) \qquad (4.28)$$

Inspecting (4.28), the frequencies of the finite attenuation poles can be determined by the capacitive load C_S and the electrical parameters of the parallel coupled-line. Fig. (4.4a) shows the pictorial descriptions of varying the capacitance C_S. There are three intersections between the upper reactance function $X_U = (Z_{oe}\tan\theta_e - Z_{oo}\tan\theta_o)/2$ and the lower one $X_L = 1/\omega C_S$ through the stopband. It means that three finite attenuation poles will be located through the stopband at the same frequencies as the intersections between the upper and lower reactance functions. As illustrated in Fig. (4.7b), the predicted results are confirmed by the simulated frequency responses. The locations of the transmission zeros are almost the same as those of the intersections shown in Fig. 4.7(a).

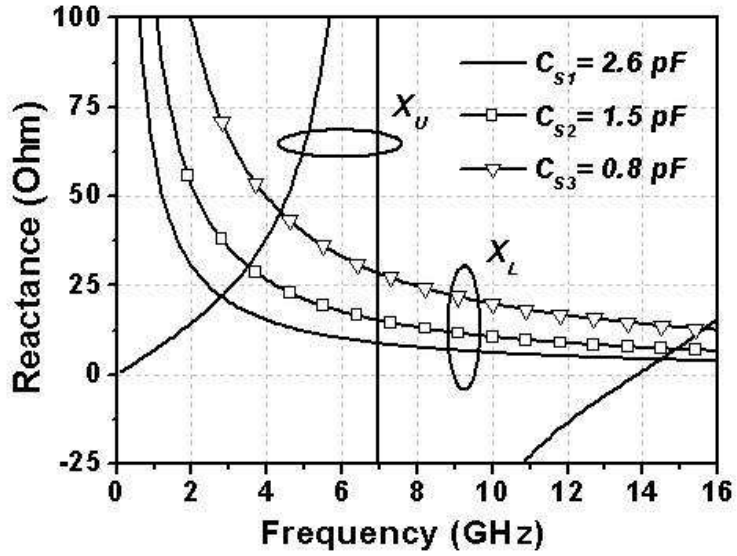

(a)

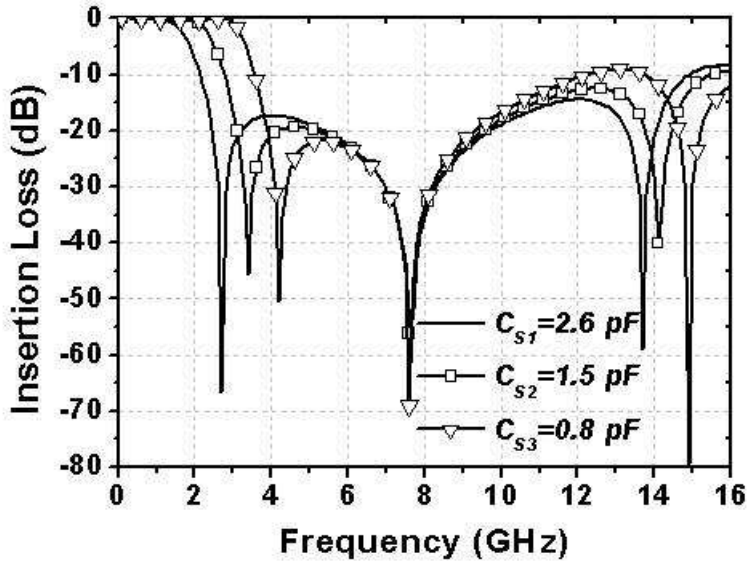

(b)

Fig. 4.7 Compact structure with different capacitive loads. (a) Pictorial reactance descriptions. (b) Simulated frequency responses with the following electrical parameters: l_c = 7.0 mm, s = 0.5 mm, and w = 0.23 mm.

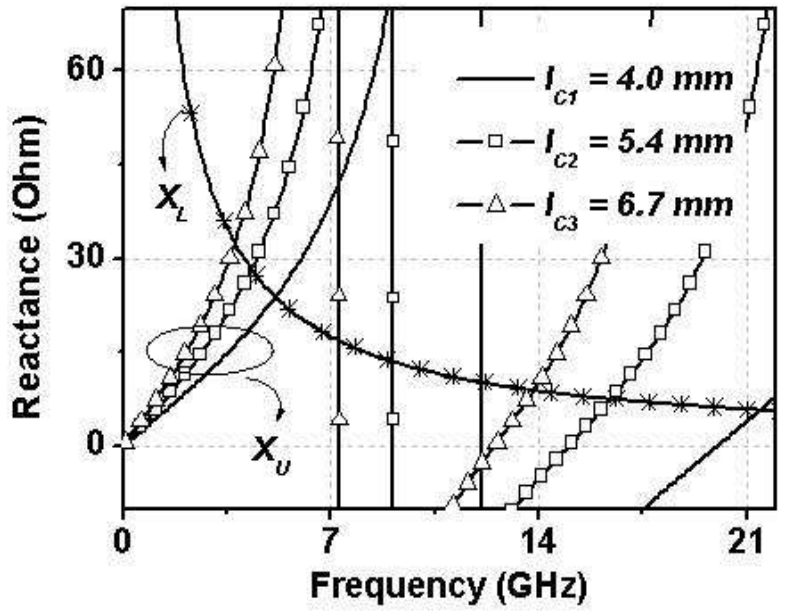
Reactance (Ohm)
60
30
0
0
7
14
21
Frequency (GHz)
X_L
X_U
l_{C1} = 4.0 mm
l_{C2} = 5.4 mm
l_{C3} = 6.7 mm

(a)

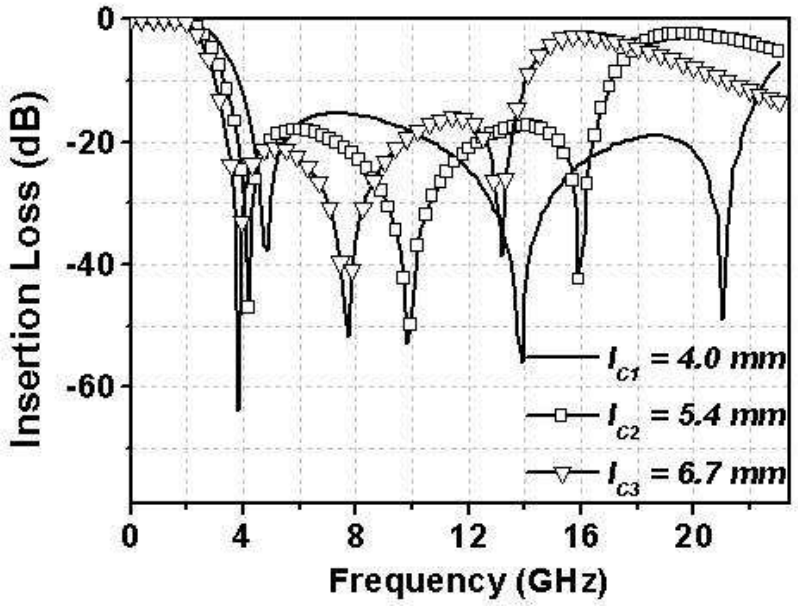
Insertion Loss (dB)
0
-20
-40
-60
0
4
8
12
16
20
Frequency (GHz)
l_{C1} = 4.0 mm
l_{C2} = 5.4 mm
l_{C3} = 6.7 mm

(b)

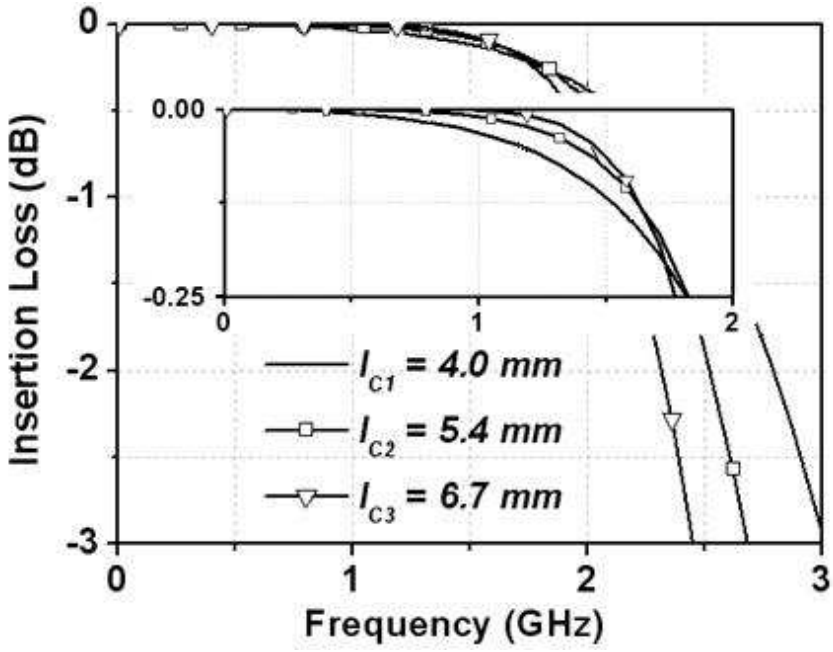

(c)

Fig. 4.8 Compact structure with different capacitive loads. (a) Pictorial reactance descriptions. (b) Simulated frequency responses with the following electrical parameters: C_S = 1.3 pF, s = 0.5 mm, and w = 0.23 mm. (c) Partial enlarged view.

The simulated results with three different capacitance values demonstrate that the first and third finite attenuation poles shift to the upper frequency as the capacitance value decreases and the second finite attenuation pole has almost no-shift. Moreover, the slope factor of the cut-off transition is about the same. Therefore, the cut-off frequency can be adjusted easily by selecting an appropriate capacitive load, but without changing the sharpness of the cut-off.

The first and second finite attenuation poles, however, will be so close as to produce just one transmission zero when the capacitance

value is selected to be small enough. To continuously inspect the effects on the frequency responses of the proposed structure caused by the parallel coupled-line, a comparison has been made among three different structures with different length of the parallel coupled-line based on same capacitive load. As shown in Fig. 4.8(a), all three intersections shift to the upper frequency as the length of the coupled-line decreases gradually, especially the second and third ones. The frequency responses demonstrated in Fig. 4.8(b) also present the same characteristics. Furthermore, from the partial enlarged view as depicted in Fig. 4.8(c), as the length of the coupled-line increases, the cut-off sharpness becomes more abrupt.

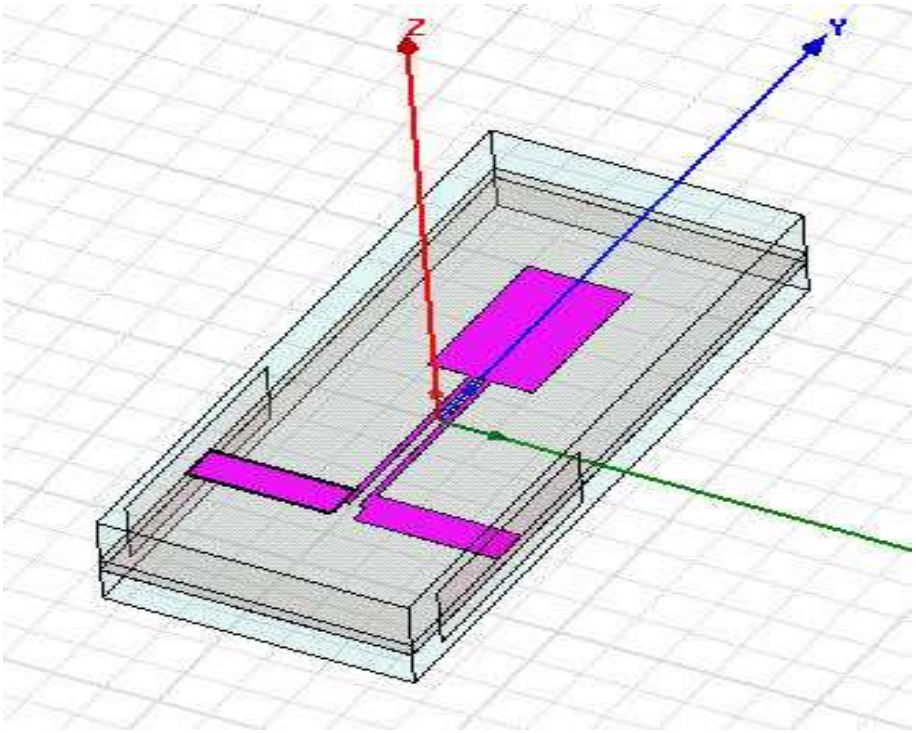

Fig. 4.9 Modeling in Ansoft HFSS simulator.

By the above graphic analysis, the proposed compact structure can provide a wide rejection band with three finite attenuation poles, and these finite attenuation poles can be adjusted easily just by changing the capacitive load value and the length of the coupled-line. This attractive feature can be used to improve the stopband characteristics of low-pass and band-pass filters for harmonics and spurious suppression. To verify the proposed approach, a low-pass filter with its cutoff frequency at 2.0 GHz is developed. The low-pass filter is designed and fabricated on a 0.76 mm thick Taconic PCB with a relative dielectric constant of ε_r = 3.5. The capacitive load can be a chip monolithic multilayered ceramic capacitor or a metal-insulator-metal capacitor. In this case, we select an open-circuited stub to be the capacitive load for simple fabrication and low insertion loss. By applying the rules examined in Section II, as well as optimized by Ansoft HFSS Simulator for considering the discontinuity effect at a step between the open-circuited stub and the parallel coupled-line, as shown in Fig. 4.9, the physical dimensions of the circuit, as depicted in Fig. 4.10(a), are determined as: l_w = 4.0 mm, l_h = 7.0 mm, l_c = 9.0 mm, w = 0.25 mm, and s = 0.36 mm. The fabricated low-pass filter is measured with Anritsu 37369D vector network analyzer. As shown in Fig. 4.10(b), the measured results agree well with the simulated ones. This low-pass filter has a 3-dB cutoff frequency at 1.99 GHz. The insertion loss is lower than 0.5 dB from DC to 1.6 GHz. The rejection band is extended from 2.7 to 8.35 GHz over 20 dB, and three finite attenuation poles are located at 3.05 GHz with 52.5 dB, at 5.45 GHz with 64.1 dB, and at 8.05 GHz with 53.0 dB, respectively.

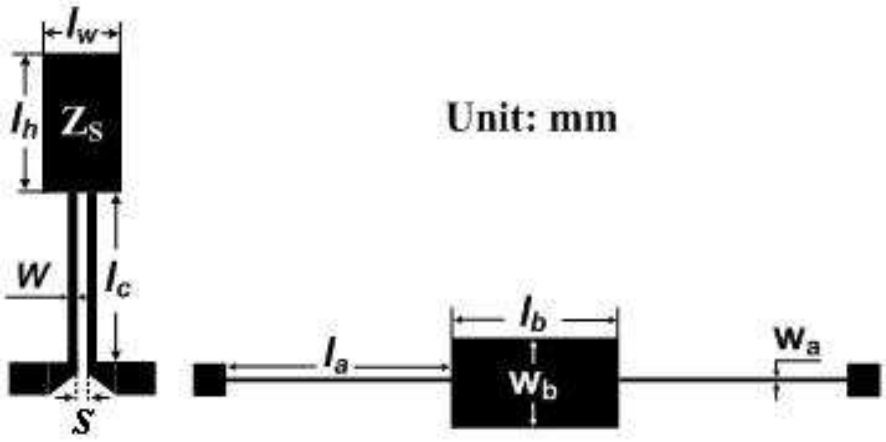

(a)

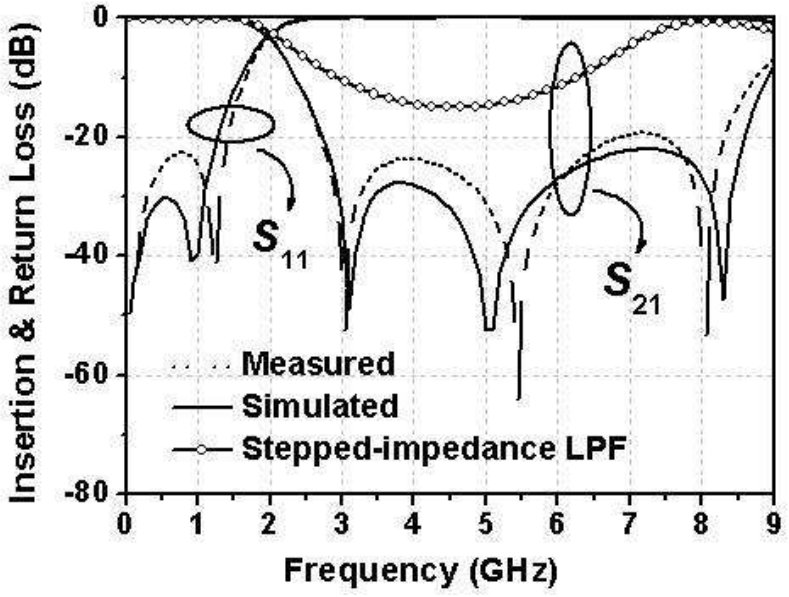

(b)

Fig. 4.10 (a) Layout comparison between the proposed and the conventional stepped-impedance LPF. (b) Simulated and measured results.

4.3 Low-pass filter with harmonics suppression

In this paper, we also develop a new kind of semi-lumped compact low-pass filter to suppress 1st, 2nd, and 3rd harmonics. In this case, a chip capacitor is used to replace the open-stub as the load capacitor in order to reduce the effective circuit area. By using the same optimizing method proposed in the fore mentioned design.

A semi-lumped low-pass filter with its cutoff frequency at 1.3 GHz is developed. The electrical parameters of the parallel coupled-line and shunted capacitor are selected to suppress the 2nd, 3rd, and 4th harmonics, simultaneously. A compact low-pass filter is designed and fabricated on a 0.76 mm thickness Taconic PCB with a relative dielectric constant of ε_r = 3.5. Adjusting the locations of the reactance intersections by adjusting the circuit parameters, as well as optimized

Table 4.1 Comparison of the physical dimensions

<table>
<tr><td colspan="2">Proposed LPF</td><td colspan="2">Stepped-impedance LPF</td></tr>
<tr><td>Coupled-line (mm)</td><td>Capacitor (pF)</td><td>High-impedance line (mm)</td><td>Low-impedance line (mm)</td></tr>
<tr><td rowspan="2">Length: 13
Width: 0.4
Space: 0.4</td><td rowspan="2">C_S : 1.5</td><td>Length: 11.51</td><td>Length: 8.45</td></tr>
<tr><td>Width: 0.22</td><td>Width: 4.54</td></tr>
<tr><td colspan="4">Substrate thickness: 0.76 mm, relative dielectric: 3.5</td></tr>
</table>

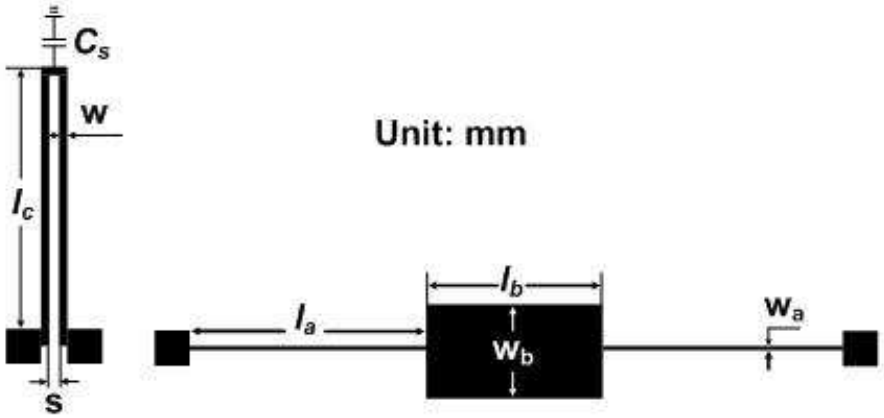

Fig. 4.11 Layouts of (a) the proposed low-pass filter and (b) conventional stepped-impedance low-pass filter.

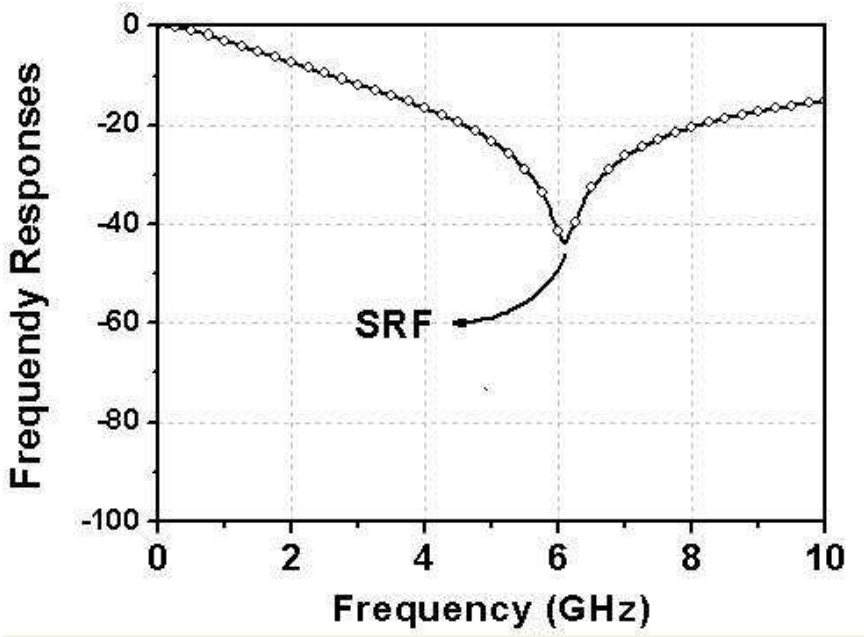

Fig. 4.12 Frequency responses of the employed load capacitor.

by Agilent ADS software, the circuit electrical parameters are determined as shown in Table 4.1, and a comparison of the circuit layouts between the proposed compact low-pass filter and the conventional stepped-impedance one has been made as illustrated in Fig. 4.11.

The employed load capacitor is a Murata product with its SRF (series resonance frequency) of 6.09 GHz. The frequency responses are investigated, as shown in Fig. 4.12. With its real frequency responses, the semi-lumped compact low-pass filter can be optimized by using commercial RF simulator tools.

A photograph of the fabricated semi-lumped low-pass filter is shown in Fig. 4.13(a). The fabricated low-pass filter was measured with Anritsu 37369D vector network analyzer. As shown in Fig. 4.13(b), the measured results agree well with the simulated ones. This low-pass filter has a 3-dB cutoff frequency at 1.3 GHz. The three finite attenuation poles at stopband are located at 2.7 GHz, 3.85 GHz, and 5.35 GHz with insertion losses of 46 dB, 47.9 dB, and 35.5 dB, respectively. The locations are almost same as the 2^{nd}, 3^{rd}, and 4^{th} harmonics of the cutoff frequency. Thereby the harmonics can be eliminated effectively.

Moreover, any of the unwanted frequencies can be eliminated using this kind of circuit by adjusting the electrical circuit parameters effectively.

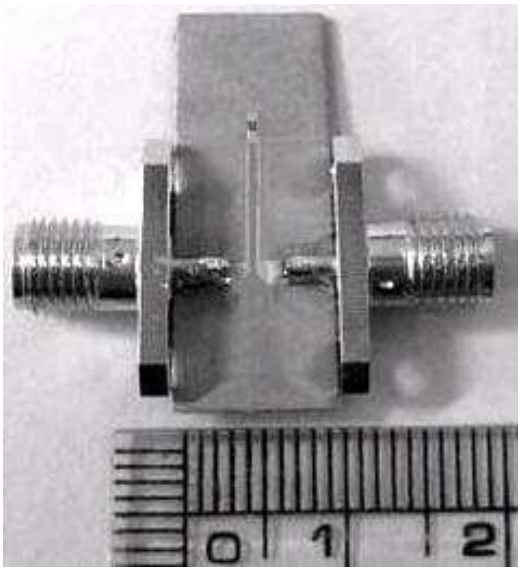

(a)

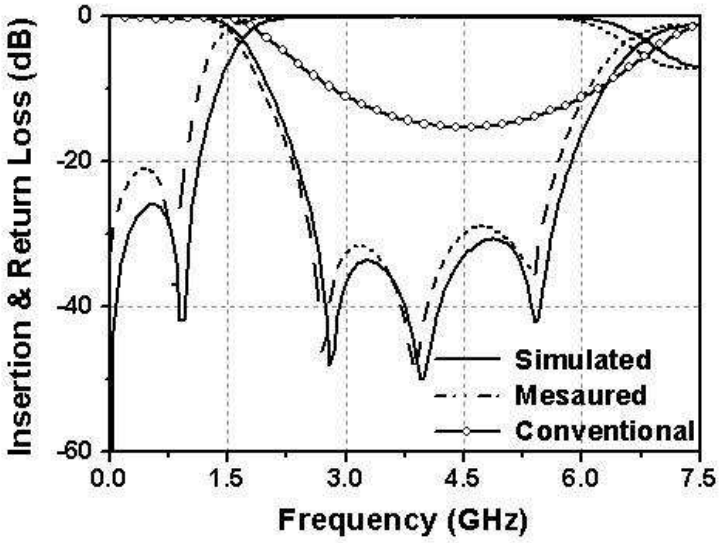

(b)

Fig. 4.13 Proposed compact low-pass filter. (a) Photograph of the fabricated circuit, (b) Measured frequency responses compared with those of the simulated and conventional stepped-impedance low-pass filter.

CHAPTER 5 Conclusions

In this dissertation, a new compact structure for improving stopband performance of low-pass filter or band-pass filter. This compact structure has many attractive advantages: very simple, easy-to-integrate, easy-to-fabricate, broad rejection bandwidth, and controllable transmission zeros for harmonic and spurious suppression.

To design this new kind of low-pass filter, two-kind of equivalent circuit comprised of lumped-elements can be an alternative. One is Chebyshev prototype, but this kind of equivalent circuit can be used just if the cutoff frequency is important not the transmission zeros for the filter's specifications. However, it's very simple and easy-to-design. The other one is a kind of equivalent circuit with a transform, by which the first transmission zero can be adjusted to meet the design requirement of skirt characteristics. In addition, a transmission-line model was proposed in this paper, by which three transmission zeros at stopband can be controlled just by adjusting the circuit electrical parameters easily. These transmission zeros can be employed to suppress harmonics and spurious signal, which are very important in modern communication system.

To verify the feasibility of the proposed method, three low-pass filters based on microstrip line structure have been designed, fabricated, and measured. Based on the observations of simulation

performance and measured results, the equivalent models have been verified. The most important thing is that a transmission-line model for this new type of compact structure was developed. By this equivalent model, three transmission zeros can be controllable completely to suppress harmonics and spurious signals. A semi-lumped low-pass filter was designed, fabricated, and measured.

This kind of low-pass filter demonstrates some desirable features compared with the conventional one, such as sharp skirt characteristics, and harmonics and spurious suppression at stopband. In addition, the proposed approach can be further extended and used in high-order design process to achieve sharper skirt characteristics and broad rejection band with much deeper attenuation level.

References

[1] Ian Hunter, *Theory and Design of Microwave Filters*, the Institution of Electrical Engineers, the United Kingdom, 2001.

[2] Jia-Sheng, Hong, M. J. Lancaster, *Microstrip Filters for RF/Microwave Applications*, John Wiley & Sons, Inc, New York, 2001.

[3] George Matthaei, Leo Young, E. M. T. Jones, *Microwave Filters, Impedance-Matching Networks, and Coupling Structures*, Norwood, MA: Artech House, 1985.

[4] Randall W. Rhea, *HF Filter Design and Computer Simulation*, Atlanta Noble Pub., 1994.

[5] I.D. Robertson and S. Lucyszyn, *RFIC and MMIC design and technology*, Randall W. Rhea, *HF Filter Design and Computer Simulation*, Atlanta Noble Pub., 1994.

[6] M. Makimoto and S. Yamashita, *Microwave Resonators and Filters for Wireless Communication*, Springer, 2001.

[7] Y. Katznelson, *An introduction to harmonics analysis 3rd edition*, Cambridge University Press, 2004.

[8] Stephen A. Maas, *Nonlinear Microwave and RF Circuits 2nd Edition*, Artech House, Feb. 2003.

[9] Eric. Bogatin, *Signal Integrity – Simplified*, Prentice Hall PTR, Sep. 2003.

[10] Tim Williams, *EMC for Product Designers*, Newnes, May, 2001.

[11] Les Besser, *Practical RF Circuit Design for Modern Wireless Systems, Volume I : Passive Circuits and Systems*, Artech House, Oct. 2003.

[12] Rowan Gilmore, *Practical RF Circuit Design for Modern Wireless Systems Vol. 2: Active Circuits and Systems*, Artech House, June. 2003.

[13] Kun-Hui Yi; Bongkoo Kang, “Modified Wilkinson power divider for nth harmonic suppression,” *IEEE Microw. and Wireless Comp.Lett. Wave Lett.*, vol. 13, no. 5, May. 2003, pp. 178-180.

[14] Wen-Hua Tu; Kai Chang; “Compact second harmonic-suppressed bandstop and bandpass filters using open stubs,” *IEEE Trans. Microw. Theory Tech.*, vol. 54, June. 2006, pp. 2497-2502.

[15] Quendo, C.; Rius, E.; Person, C.; Ney, M., “Integration of optimized low-pass filters in a bandpass filter for out-of-band improvement,” *IEEE Trans. Microw. Theory Tech.*, vol. 49, Dec 2001, pp. 2376-2383.

[16] I. Rumsey, M. Piket-May, and P. K. Kelly, “Photonic Bandgap Structure used as Filters in Microstrip Circuits,” *IEEE Microw. Guided Wave Lett.*, vol. 8, no. 10, Oct. 1998, pp. 336-338.

[17] D. Ahn, J. S. Park, C. S. Kim, J. Kim, Y. Qian, and T. Itoh, “A Design of the Low-Pass Filter Using the Novel Microstrip Defected Ground Structure,” *IEEE Trans. Microw. Theory Tech.*, vol. 49, Jan. 2001, pp. 86-93.

[18] Jyh-Wen Sheen, "A Compact Semi-Lumped Low-Pass Filter for Harmonics and Spurious Suppression," IEEE Microw. Guided Wave Lett., vol. 10, Mar. 2000, pp. 92-93

[19] Joseph F. White, *High Frequency Techniques: An Introduction to RF and Microwave Engineering*, Wiley-IEEE Press, Oct. 2004.

[20] L.-H Hsieh and K. Chang, “Compact Low-pass Filter Using Stepped Impedance Hairpin Resonator,” *Electron. Lett.* vol. 10, Mar. 2000, pp. 92-93.

[21] L.-H Hsieh and K. Chang, “Compact Elliptic-Function Low-pass Filters Using Microstrip Stepped-Impedance Hairpin Resonators,” *IEEE Microw. Theory Tech.*, vol. 51, Jan. 2003, pp. 193-199.

[22] Kun-Hui Yi; Bongkoo Kang, “Compact Microstrip Low-pass Filter With Sharp Rejection Characteristics,” *IEEE Microw. and Wireless Comp.Lett. Wave Lett.*, vol. 13, no. 5, May. 2003, pp. 178-180.

[23] Stephen Butterworth, “On the Theory of Filter Amplifiers,” *Wireless Engineer* (also called *Experimental Wireless and the Radio Engineer*), vol. 7, 1930, pp. 536-541.

[24] David M. Pozar, *Microwave Engineering 3rd edition*, John Wiley & Sons, Inc, 2005.

[25] Inder Bahl, *Lumped Elements for RF and Microwave Circuits*, Artech House, 2003.

[26] J. Helszajn, *Passive and active Microwave Circuits*, Heriot-Watt University vEdinburgh, United Kingdom, 1979.

[27] J. A. G. Malherbe, *Microwave Transmission Line Couplers*, Artech House, Inc., 1988.

[28] K.C. Gupta, R. Garg, I. Bahl, and P. Bhartia, *Microstrip Lines and Slotlines* 2nd edition, Artech House, 1996.

[29] Lap Kun Yeung and Ke-Li Wu, “A Compact Second-Order LTCC Bandpass Filter With Two Finite Transmission Zeros,” *IEEE Microw. Theory Tech.*, vol. 51, Feb. 2003, pp. 337-341.

[30] Chun-Fu Chang and Shyh-Jong Chung, “Bandpass Filter of Serial Configuration With Two Finite Transmission Zeros Using LTCC Technology,” *IEEE Microw. Theory Tech.*, vol. 53, July. 2005, pp. 2383-2388.

[31] David H. Schrader and, *Microstrip Circuit Analysis*, Prentice Hall, 1995.

[32] Robert E. Collin, *Foundations for Microwave Engineering*, McGraw-Hill, 1995.

Appendix I S, ABCD, Y, and Z parameters

	ABCD	*Y*	*Z*
S_{11}	$\frac{A + B/Z_0 - CZ_0 - D}{A + B/Z_0 + CZ_0 + D}$	$\frac{(Y_0 - Y_{11})(Y_0 + Y_{22}) + Y_{12}Y_{21}}{(Y_0 + Y_{11})(Y_0 + Y_{22}) - Y_{12}Y_{21}}$	$\frac{(Z_{11} - Z_0)(Z_{22} + Z_0) - Z_{12}Z_{21}}{(Z_{11} + Z_0)(Z_{22} + Z_0) - Z_{12}Z_{21}}$
S_{12}	$\frac{2(AD - BC)}{A + B/Z_0 + CZ_0 + D}$	$\frac{-2Y_{12}Y_0}{(Y_0 + Y_{11})(Y_0 + Y_{22}) - Y_{12}Y_{21}}$	$\frac{2Z_{12}Z_0}{(Z_{11} + Z_0)(Z_{22} + Z_0) - Z_{12}Z_{21}}$
S_{21}	$\frac{2}{A + B/Z_0 + CZ_0 + D}$	$\frac{-2Y_{21}Y_0}{(Y_0 + Y_{11})(Y_0 + Y_{22}) - Y_{12}Y_{21}}$	$\frac{2Z_{21}Z_0}{(Z_{11} + Z_0)(Z_{22} + Z_0) - Z_{12}Z_{21}}$
S_{22}	$\frac{-A + B/Z_0 - CZ_0 + D}{A + B/Z_0 + CZ_0 + D}$	$\frac{(Y_0 + Y_{11})(Y_0 - Y_{22}) + Y_{12}Y_{21}}{(Y_0 + Y_{11})(Y_0 + Y_{22}) - Y_{12}Y_{21}}$	$\frac{(Z_{11} + Z_0)(Z_{22} - Z_0) - Z_{12}Z_{21}}{(Z_{11} + Z_0)(Z_{22} + Z_0) - Z_{12}Z_{21}}$

(*b*) *ABCD* parameters in terms of *S*, *Y*, and *Z* parameters

	S	*Y*	*Z*
A	$\frac{(1 + S_{11})(1 - S_{22}) + S_{12}S_{21}}{2S_{21}}$	$\frac{-Y_{22}}{Y_{21}}$	$\frac{Z_{11}}{Z_{21}}$
B	$Z_0 \frac{(1 + S_{11})(1 + S_{22}) - S_{12}S_{21}}{2S_{21}}$	$\frac{-1}{Y_{21}}$	$\frac{Z_{11}Z_{22} - Z_{12}Z_{21}}{Z_{21}}$
C	$\frac{1}{Z_0} \frac{(1 - S_{11})(1 - S_{22}) - S_{12}S_{21}}{2S_{21}}$	$\frac{-(Y_{11}Y_{22} - Y_{12}Y_{21})}{Y_{21}}$	$\frac{1}{Z_{21}}$
D	$\frac{(1 - S_{11})(1 + S_{22}) + S_{12}S_{21}}{2S_{21}}$	$\frac{-Y_{11}}{Y_{21}}$	$\frac{Z_{22}}{Z_{21}}$

(*c*) *Y* parameters in terms of *S*, *ABCD*, and *Z* parameters

	S	*ABCD*	*Z*
Y_{11}	$Y_0 \frac{(1 - S_{11})(1 + S_{22}) + S_{12}S_{21}}{(1 + S_{11})(1 + S_{22}) - S_{12}S_{21}}$	$\frac{D}{B}$	$\frac{Z_{22}}{Z_{11}Z_{22} - Z_{12}Z_{21}}$
Y_{12}	$Y_0 \frac{-2S_{12}}{(1 + S_{11})(1 + S_{22}) - S_{12}S_{21}}$	$\frac{-(AD - BC)}{B}$	$\frac{-Z_{12}}{Z_{11}Z_{22} - Z_{12}Z_{21}}$
Y_{21}	$Y_0 \frac{-2S_{21}}{(1 + S_{11})(1 + S_{22}) - S_{12}S_{21}}$	$\frac{-1}{B}$	$\frac{-Z_{21}}{Z_{11}Z_{22} - Z_{12}Z_{21}}$
Y_{22}	$Y_0 \frac{(1 + S_{11})(1 - S_{22}) + S_{12}S_{21}}{(1 + S_{11})(1 + S_{22}) - S_{12}S_{21}}$	$\frac{A}{B}$	$\frac{Z_{11}}{Z_{11}Z_{22} - Z_{12}Z_{21}}$

(*d*) *Z* parameters in terms of *S*, *ABCD*, and *Y* parameters

	S	*ABCD*	*Y*
Z_{11}	$Z_0 \frac{(1 + S_{11})(1 - S_{22}) + S_{12}S_{21}}{(1 - S_{11})(1 - S_{22}) - S_{12}S_{21}}$	$\frac{A}{C}$	$\frac{Y_{22}}{Y_{11}Y_{22} - Y_{12}Y_{21}}$
Z_{12}	$Z_0 \frac{2S_{12}}{(1 - S_{11})(1 - S_{22}) - S_{12}S_{21}}$	$\frac{(AD - BD)}{C}$	$\frac{-Y_{12}}{Y_{11}Y_{22} - Y_{12}Y_{21}}$
Z_{21}	$Z_0 \frac{2S_{21}}{(1 - S_{11})(1 - S_{22}) - S_{12}S_{21}}$	$\frac{1}{C}$	$\frac{-Y_{21}}{Y_{11}Y_{22} - Y_{12}Y_{21}}$
Z_{22}	$Z_0 \frac{(1 - S_{11})(1 + S_{22}) + S_{12}S_{21}}{(1 - S_{11})(1 - S_{22}) - S_{12}S_{21}}$	$\frac{D}{C}$	$\frac{Y_{11}}{Y_{11}Y_{22} - Y_{12}Y_{21}}$

Appendix II Useful two-port networks

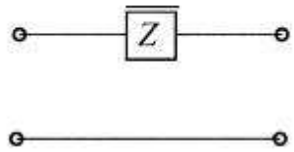

$$A = 1 \quad B = Z$$
$$C = 0 \quad D = 1$$

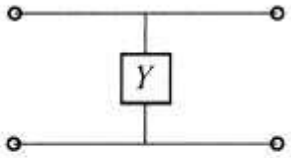

$$A = 1 \quad B = 0$$
$$C = Y \quad D = 1$$

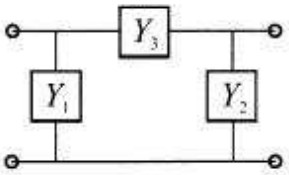

$$A = 1 + \frac{Y_2}{Y_3} \qquad B = \frac{1}{Y_3}$$
$$C = Y_1 + Y_2 + \frac{Y_1 Y_2}{Y_3} \qquad D = 1 + \frac{Y_1}{Y_3}$$

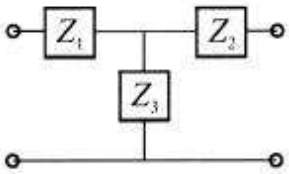

$$A = 1 + \frac{Z_1}{Z_3} \qquad B = Z_1 + Z_2 + \frac{Z_1 Z_2}{Z_3}$$
$$C = \frac{1}{Z_3} \qquad D = 1 + \frac{Z_2}{Z_3}$$

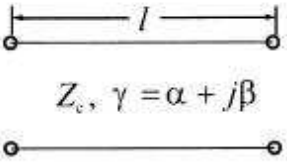

$$A = \cosh\gamma l \qquad B = Z_c \sinh\gamma l$$
$$C = \frac{\sinh\gamma l}{Z_c} \qquad D = \cosh\gamma l$$

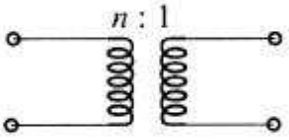

$$A = n \quad B = 0$$
$$C = 0 \quad D = \frac{1}{n}$$

Published papers Concerned with this dissertation

1 Domestic Conference & Journal

[1] 김동일, 김보영, and Rui Li, “링 공진기를 사용한 대역통과 필터의 설계에 관한 연구,” *해사산업연구소논문집*, vol. 21, pp. 79-84, Jan. 2004.

[2] 김동일, 김보영, and Rui Li, “링 공진기를 사용한 대역통과 필터의 설계에 관한 연구”, *한국전자파학회지*, vol. 15, no. 6, pp. 533-539, Jun. 2004.

[3] 김동일, Rui Li, 정상욱, 전중성, and 최동묵, “Modified 3 dB Branch Line Coupler for Harmonic Waves Suppression," *산업기술연구소 학술강연회 논문집*, pp. 42-48, Aug. 2004.

[4] 김동일, 정상욱, 김민정, 장신자, and Rui Li, “PC 용 광대역 EMC 필터의 성능 개선,” *산업기술연구소 학술강연회 논문집*, pp. 36-41, Aug. 2004.

[5] Dong Il Kim and Rui Li, “Design for Harmonic Waves Suppression Based on 3 dB Branch Line Coupler," *해사산업연구소논문집*, vol. 15, pp. 55-60, Sep. 2004.

[6] Dong Il Kim, Rui Li, Seung Jae Shin, and Sang Hyun Moon, “Modified 3dB Branch Line Coupler for Harmonic Wave Suppression,” *추계 마이크로파 및 전파학술대회 논문집*, pp. 315-318, Sep. 2004.

[7] Seung Jae Shin, Sang Hyun Moon, Dong Il Kim, Jae Man Song, and Rui Li, “Development of Electromagnetic Wave Absorbers,” *추계 마이크로파 및 전파학술대회 논문집*, pp. 496-499, Sep. 2004.

[8] 전중성, Rui Li, and 김동일, “A Study on Linearization of Inter-modulation Distortion for IMT-2000," *산업기술연구소 학술강연회 논문집*, pp. 35-47, Mar. 2005.

[9] 최창묵, 김동일, Rui Li, and 오경진, “RCS 법에 의한 전파흡수체 측정기법 분석”, *전자파기술 하계 학술대 회 논문집*, vol. 5, No. 1, pp. 159-162, Jun. 2005.

[10] Rui Li, Dong Il Kim, and Joong Sung Jeon, “Compact Low-Pass Filter for Harmonics and Spurious Suppression,” *산업기술연구소 학술강연회 논문집*, pp. 45-49, May 2006.

[11] Rui Li, Dong Il Kim, and Chang-Mook Choi, “Semi-Lumped Low-Pass Filter for Harmonics Suppression,” *Journal of the Korea Electromagnetic Engineering Society,* Oct. 2006.

1 International Conference & Journal

[1] Rui Li, Dong Il Kim, and Chang-Mook Choi, “Compact Low-Pass Filter with Sharp Skirt Characteristics and Broad Stopband,” International Journal of Navigation and Port Research, pp. 607-610, Sep. 2006.

[2] Rui Li and Dong Il Kim, “A New Compact Low-Pass Filter with Broad Stopband and Sharp Skirt Characteristics,” Asia-Pacific

Microwave Conference 2005, Suzhou China, vol. 3, pp. 1450-1452, Dec. 2005.

[3] Rui Li and Dong Il Kim, and Chang-Mook Choi, "A Novel Compact Low-Pass Filter and Its Equivalent Circuit," Asia Navigation Conference 2006, Jezu, Korea, pp. 79-84, Oct. 2006.

[4] Chang-Mook Choi, Dong Il Kim, Dong-Han Choi, and Rui Li, "Development of Broad-Band Electromagnetic Wave Absorber for X-band Sensors in Double-layered Type Using Carbon," 12th IAIN World Congress 2006 International Symposium on GPS/GNSS, pp. 297-300, Oct. 2006.

[5] Dong-Han Choi, Dong Il Kim, Chang-Mook Choi, and Rui Li, "A Study on Multi-layered EM Wave Absorber Using Natural Lacquer as a Binder," 12th IAIN World Congress 2006 International Symposium on GPS/GNSS, pp. 157-161, Oct. 2006.

[6] Rui Li, Dong Il Kim, and Chang-Mook Choi, "Compact Structure with Three Attenuation Poles for Improving Stopband Characteristics," IEEE Microwave and Wireless Components Letters, Dec. 2006.

[7] Rui Li, Dong Il Kim, and Chang-Mook Choi, "Compact Low-Pass Filter for Harmonics Suppression," Asia-Pacific Microwave Conference 2006, Yokohama, Japan, Dec. 2006.

Acknowledgement

I would like to thank many people who have helped me during the past four years. Without their supports and encouragements, it is impossible for me to finish this dissertation.

I am deeply grateful to my advisor, Professor Dong Il Kim. His wide knowledge, strict research attitude and enthusiasm in work deeply impressed me and taught me what a true scientific research should be. I am also thankful to the other Professors of our department for their supports and guidance on this work, who are Professor Hyung Rae Cho, Professor Kyeong-Sik Min, Professor In-ho Kang, Professor Ki Man Kim, Professor Ji Won Jung, Professor Young Yun. In addition, I am thankful to Dr. Young-Su Weon who is the Director of KNN, and Dr. Woo Keun Park who is the Minister of KBS Busan for their generous help and encouragement.

I greatly appreciate the constructive comments and helpful suggestions received from referees that helped me in preparing significantly improved and modified version of this dissertation.

Certainly, I cannot be thankful enough to our laboratory members for their timely and unselfish help. They not only help me my research work, but also let me enjoy the friendly work environment and they teach me Korean at anytime when I need. So I have many thanks to Dr. Jun-Young Son, Dr. Dong-Han Choi and Mr. Chang-Mook Choi they have been doing excellent work in EM wave absorbers research area ,

and the other friends in my lab, they are Mr. Seung-Hun Che, Mr. Yun-Seok Choi, Mr. Je-Hun Lee, etc. Also, I would like to thank Miss Sang-Mee Park for her kindness and generous help to me.

I would like to appreciate some friends who are from China and studying in our university, Mr. Shi-Wei Shan, Mr. Xu-Guang Wang they are working toward M.S in the same department with me, and Dr. Yong-Nam Park, Dr. Moon-Jin Park, etc. for their continuous support and encouragement, especially during the hard times of mine.

Especially, I would express my sincere thanks to Professor Man-Hong Kim at the Dalian Maritime University, China. Without his help, it is impossible for me to get this great opportunity to study in Korea.

This dissertation is dedicated to my families and my girl friend, Cai-rong Zheng, for their support and love.